Active control of resistive wall mode via modification of external tearing index

Yuling He, Yueqiang Liu, Xu Yang, Guoliang Xia, and Li Li

View Online   Export Citation   CrossMark

Active control of resistive wall mode via modification of external tearing index

Yuling He,[1,2] (ID) Yueqiang Liu,[3] (ID) Xu Yang,[4] Guoliang Xia,[5] and Li Li[6,a]

AFFILIATIONS

[1]Guangdong Provincial Key Laboratory of Quantum Engineering and Quantum Materials, School of Physics and Telecommunication Engineering, South China Normal University, Guangzhou 510006, China
[2]Guangdong-Hong Kong Joint Laboratory of Quantum Matter, South China Normal University, Guangzhou 510006, China
[3]General Atomics, P.O. Box 85608, San Diego, California 92186-5608, USA
[4]Chongqing Engineering Laboratory for Detection, Control and Integrated System, Chongqing Technology and Business University, Chongqing 400067, China
[5]CCFE, Culham Science Centre, Abingdon OX14 3DB, United Kingdom
[6]College of Science, Donghua University, Shanghai 201620, China

[a]Author to whom correspondence should be addressed: heyl@m.scnu.edu.cn

ABSTRACT

Modification of the external tearing index, Δ'_{ext}, by magnetic feedback is analytically investigated for the purpose of controlling the resistive plasma resistive wall mode (RP-RWM). The matching method is pursued by deriving expressions for the close-loop Δ'_{ext} and by linking it to the counterpart from the inner layer. Various feedback coil configurations are found to generally reduce Δ'_{ext} and stabilize the RWM, with either proportional or derivative control. Feedback modification of Δ'_{ext} is found to be generally independent of the inner layer resistive interchange index D_R, confirming that feedback action primarily modifies the solution in the outer ideal region for the RP-RWM. Exception occurs when either the inner layer favorable curvature effect becomes sufficiently large or the feedback action is sufficiently strong to introduce a rotating RP-RWM in the static plasma, leading to complex-valued close-loop Δ'_{ext}. The perturbed magnetic energy dissipation in the outer region, associated with the eddy current in the resistive wall, is identified as the key physics reason for feedback induced complex Δ'_{ext}. Similar results are also obtained for active control of the external kink instability, whose open-loop growth rate is significantly reduced by inclusion of the plasma resistivity. Within the single poloidal harmonic approximation, which is most suitable for the matching approach, external active coils combined with poloidal sensors are often found to be more efficient for feedback stabilization of the mode at large proportional gain values. This counter-intuitive result is explained as the lack of (non-resonant) poloidal harmonics for proper description of the feedback coil geometry.

Published under license by AIP Publishing. https://doi.org/10.1063/5.0019233

I. INTRODUCTION

Magneto-hydrodynamic (MHD) instabilities, such as the external kinks (EK) and (neoclassical) tearing modes ((N)TM), are major concerns for high pressure advanced tokamaks (AT).[1] Within a certain pressure limit, the EK can be stabilized by a perfectly conducting wall located sufficiently close to the plasma edge.[2] However, the wall has finite conductivity in reality, which allows the leakage of the radial magnetic flux perturbation through the wall on long time scale. The resulting residual instability is called the resistive wall mode (RWM). The RWM often limits the operational space of advanced tokamaks because such a low-n (n is the toroidal mode number) macroscopic

instability sets a beta (β) limit for the AT operation.[3] Here $\beta = 2\mu_0 \langle p \rangle / \boldsymbol{B}^2$ is the ratio of the volume averaged plasma pressure to the magnetic pressure. In order to maximize the benefit of the AT scenario, such as that foreseen in ITER,[1] the RWM needs to be stabilized.

Numerical and analytical calculations,[4–9] based on the ideal MHD model, indicate that stabilization of the ideal plasma RWM (IP-RWM) can be achieved by certain free energy dissipation mechanism(s) inside the plasma in the presence of toroidal plasma rotation. The critical rotation frequency for a complete stabilization of the mode was predicted to be several percent of the Alfvén frequency. However, early work[10–12] employing the resistive MHD model showed

that the toroidal curvature effect, associated with the resistive layer near the rational surfaces, can stabilize the resistive-plasma RWM (RP-RWM), though with the stability window being narrow in toroidal geometry. More recent studies indicated that a slow plasma rotation flow, with the flow speed several times larger than the typical tearing mode growth rate, in combination with the resistivity layer induced energy dissipation, can stabilize the RP-RWM.[13–15]

Plasmas in future reactors are expected to rotate with low or negligible speed. Therefore, active control of the plasma instability in the absence of flow is of particular interest. Active control of the RWM has been studied for both resistive and ideal plasma models,[16–21] showing that a magnetic feedback system, combined with the slow plasma flow, can stabilize the mode. Reference 22 studied direct feedback stabilization of the resistive plasma (tearing-like) modes utilizing magnetic coils in a cylindrical plasma. The results presented in Ref. 22 show that magnetic feedback can stabilize a resistive mode even when the open-loop is unstable with an ideal wall. Reference 23 considered the effects of complex feedback gains and plasma rotation. Active control of the mode was found possible well above the ideal wall limit and with finite plasma rotation.

Recently, experimental results on magnetic feedback control of the RWM were reported in several devices, including RFX-mod,[24] KSTAR,[25] JT-60SA,[26] and DIII-D with discharges simulating the ITER baseline scenario.[27] Feedback stabilization of the mode was found (or projected to be) possible in all these devices.

This work differs from the previous analytic theory[22,23] in several aspects: (i) the explicit utilization of the matching method, (ii) a systematic investigation of various feedback configurations, and (iii) consideration of resistive layer physics with (vs without) the favorable average curvature effect.

In analytic theory, active control of the RWM is often studied relying on the plasma response model (PRM),[28–30] which is suitable for studying feedback control of the IP-RWM. In contrast, study of the RP-RWM is conventionally analyzed by proper matching procedures.[31] The matching approach is similar to the analysis employed for studying the TM by separately solving the MHD equations in the inner resistive layer and in the outer ideal bulk region.[32] The matching condition often involves a key parameter Δ' (the tearing index) from both the internal and external solutions. The external tearing index, Δ'_{ext}, is defined as the logarithmic derivative jump of the perturbed radial magnetic field across the mode resonant surface. In more general cases, the outer-region solution possesses regular singularities at the rational surface, with two independent solutions called small and big solutions that exhibit different fractional power-like asymptotic behaviors. The ratio of the leading Frobenius coefficients of the small to big solutions is defined as Δ'_{ext}.[33] A recent study has shown that this tearing index can be modified by a simple magnetic feedback,[34] without considering the role played by the resistive wall. The external tearing index is matched to that from the resistive layer solution to obtain the final dispersion relation for the RP-RWM. It is expected that stability of the RP-RWM can be modified by actively controlling the external tearing mode index Δ'_{ext}—a venue pursued in this work.

In this work, we carry out analytic study of feedback stabilization of the RWM via the matching approach, based on a cylindrical plasma model. We investigate feedback modification of Δ'_{ext} while systematically considering various choices of the feedback coil configuration. Although the focus of this work is on the RWM, the approach

exploited here is also applicable for controlling stability of the tearing mode.

In Sec. II, we present the details of our analytic model on feedback modification of Δ'_{ext}. In Sec. III, we investigate feedback stabilization of the IP-RWM via modification of Δ'_{ext} and compare the results with that from the PRM approach. Based on the matching approach, Sec. IV reports the feedback study for the RP-RWM with or without the favorable average curvature effect (i.e., the GGJ effect discovered by Glasser, Green, and Johnson[33]). Inspired by Finn's work,[22] we also carry out a similar study on the resistive plasma external kink (RP-EK) mode, following the matching approach in Sec. V. All the aforementioned studies are carried out assuming a simple proportional feedback controller, with additional results assuming a proportional–derivative (PD) controller reported in Appendix C. Section VI draws conclusions.

II. ANALYTIC MODEL

Our analytic model is based on a cylindrical circular plasma. In what follows, we start by describing the open-loop model, followed by the closed-loop model with the feedback coils.

A. Open-loop model

In the cylindrical geometry, we consider the linearized, Newcomb-like equation with finite plasma pressure in the outer region[11]

$$-\frac{\gamma^2}{F} \nabla_\perp \cdot \left(\rho \nabla_\perp \frac{\psi}{F} \right) = \frac{1}{r}\frac{d}{dr}\left(r\frac{d\psi}{dr} \right) - \frac{m^2}{r^2}\psi - \frac{m}{rF}\frac{dJ_z}{dr}\psi$$
$$- \frac{2m^2 B_\theta^2}{r^3 B_z^2 F^2}\frac{dP}{dr}\psi, \tag{1}$$

where r and θ are the radial coordinate and the poloidal angle of the plasma cross section, respectively. J_z is the plasma equilibrium density along the cylinder and P is the equilibrium pressure. γ is the eigenvalue of the instability (the RWM in our case). ψ is the m th poloidal harmonic of the perturbed poloidal magnetic flux function, which has an $\exp(im\theta - ikz) = \exp(im\theta - in\phi)$ variation, where $k = n/R_0$ with n being the toroidal mode number, and R_0 is the equivalent major radius. $F \equiv mB_\theta - kB_z$, with $\mathbf{B} = B_\theta\hat{\theta} + B_z\hat{z}$ being the equilibrium field. Finally, the operator $\nabla_\perp$ is defined as $\nabla_\perp^2\psi \equiv \frac{1}{r}(r\psi')' - \frac{m^2}{r^2}\psi$.

Simplified equilibrium radial profiles are assumed, as shown in Fig. 1. The equilibrium current density $J_z(r)$ is a step function with $J_z = J_0 = const$ at $0 \le r < r_0$ and $J_z = 0$ at $r_0 < r \le a$. The plasma equilibrium pressure is assumed to be constant, $P = P_0 = const$, across the whole plasma column. The toroidal equilibrium field is also assumed to be a constant. As a result, the radial profile of the safety factor, $q(r)$, is a constant $q = q_0$ at $0 \le r < r_0$ and a parabolic function at $r_0 < r \le a$. The parameters are chosen such that only one resonant surface is present inside the plasma for the $n = 1$ perturbation.

The Laplace equation $\nabla_\perp^2\psi \equiv 0$ is satisfied everywhere inside and outside the plasma region, except at the radial points $r = r_0$, a, r_w, where r_w denotes the resistive wall minor radius. The jump conditions for the radial derivative of the flux function ψ can be easily obtained, by integrating Eq. (1) across the above discrete radial points. We have
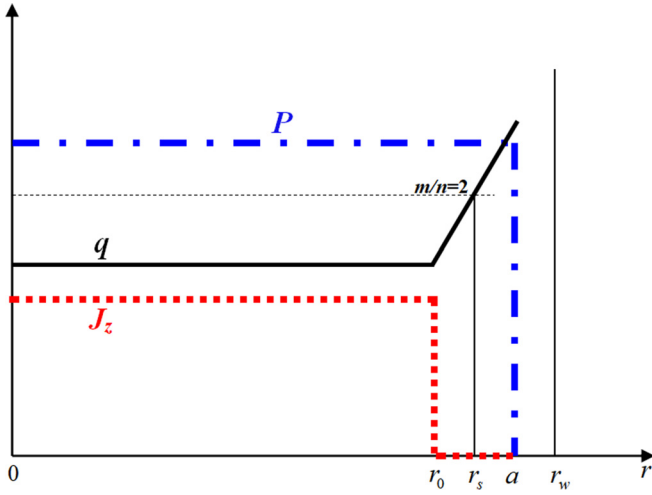
FIG. 1. The equilibrium profiles of the plasma pressure P, the axial current density J_z, and the safety factor q. One rational surface $q = m/n = 2$ ($n = 1$) is located inside the plasma.

$$\left.\frac{r[\psi']}{\psi}\right|_{r_0} = -\frac{2m}{m - nq_0}, \tag{2}$$

$$\left.\frac{r[\psi']}{\psi}\right|_{a} = -\frac{\beta m^2}{(m - nq_a)^2}, \tag{3}$$

$$\left.\frac{r[\psi']}{\psi}\right|_{r_w} = \gamma\tau_w, \tag{4}$$

where $\beta = 2\mu_0 P_0 / B_z^2$ is the ratio of the plasma pressure to the magnetic pressure, $q_a = q_0(a/r_0)^2$ is the safety factor value at the plasma surface, and $\tau_w = \mu_0 r_w d_w / \eta_w$ characterizes the magnetic flux diffusion time through the resistive wall, with d_w and η_w denoting the wall thickness and resistivity, respectively.

The solution of the Laplace equation satisfies the following relation between any two discrete points r_1 and r_2, provided that the solution is smooth within the interval (r_1, r_2):

$$\frac{1 + \left.\frac{1}{m}\frac{r\psi'}{\psi}\right|_{r_1+}}{1 - \left.\frac{1}{m}\frac{r\psi'}{\psi}\right|_{r_1+}} = \left(\frac{r_1}{r_2}\right)^{2m} \frac{1 + \left.\frac{1}{m}\frac{r\psi'}{\psi}\right|_{r_2-}}{1 - \left.\frac{1}{m}\frac{r\psi'}{\psi}\right|_{r_2-}}. \tag{5}$$

The above relation helps to connect different regions separated by the jump conditions (2)–(4). With the additional conditions of $r\psi'/\psi|_{r_0-} = m$ and $r\psi'/\psi|_{r_w+} = -m$, one can derive the jump of the logarithmic derivative $\Delta'_{\text{ext}} \equiv [\psi'(r_s+) - \psi'(r_s-)]/\psi(r_s)$ across the mode rational surface r_s,

$$\Delta'_{\text{ext}} = -\frac{2m}{r_s}\left[\frac{B}{\alpha_s + (1-\alpha_s)B} - \frac{A}{\alpha_0 + (1-\alpha_0)A}\right], \tag{6}$$

where $B = \frac{1}{1-\alpha_w \alpha_{rw}} - \hat{\beta}$ with $\alpha_{rw} = \frac{\gamma\tau_w}{\gamma\tau_w + 2m}$, and $A = A_0 - (\gamma\tau_A)^2 A_1$ with $A_0 = \frac{1}{m - nq_0}$ and $A_1 = \frac{q_0^2}{2(m-nq_0)^2}$, with the latter often being a negligible inertia term for the RWM. The additional notations are defined

as $\hat{\beta} \equiv \frac{m\beta}{2(m-nq_a)^2}$, $\alpha_w \equiv a^{2m}/r_w^{2m}$, $\alpha_s \equiv r_s^{2m}/a^{2m}$ and $\alpha_0 \equiv r_s^{2m}/r_0^{2m}$. Note that Δ'_{ext} here is defined as the external tearing index within the so-called constant-ψ approximation. Expression (6) is the value of Δ'_{ext} in the absence of any active control. The growth rate of the open-loop IP-RWM can be obtained by setting $\Delta'_{\text{ext}} = 0$.

B. Close-loop with proportional feedback

A magnetic feedback system consists of sensor coils, active coils, and control logic. We consider three types of sensors (all located at the wall radius r_w). One is the radial sensor, with the sensor signal y defined as the radial flux $\psi(r_w)$ at the wall radius. The other two, the external poloidal sensor and the internal poloidal sensor, are defined as $y = -r\psi'|_{r_w+}$ and $y = -r\psi'|_{r_w-}$, respectively. Furthermore, we consider two types of active coils, defined by their relative radial location to the wall. For the active coils located outside the wall, $r_w < r_f$, the field solution can be written as $\psi(r) = \psi_f(\frac{r}{r_w})^m + c(\frac{r}{r_w})^{-m}$ in the vacuum region $r_w < r < r_f$, where $\psi_f \equiv \psi_f(r_w)$ is the free-space field at the wall radius and produced by the active coil current solely. For the active coils located between the plasma surface and the wall, $a < r_f < r_w$, the field solution can be written as $\psi(r) = \alpha_f \psi_f(\frac{r}{r_w})^m + c_1(\frac{r}{r_w})^m + c_2(\frac{r}{r_w})^{-m}$, with $\alpha_f \equiv r_w^{2m}/r_f^{2m}$, in the vacuum region $a < r < r_f$ and $\psi(r) = \psi_f(\frac{r}{r_w})^{-m} + c_1(\frac{r}{r_w})^m + c_2(\frac{r}{r_w})^{-m}$ in the vacuum region $r_f < r < r_w$.

The simplest feedback logic is $\psi_f = -Ky$, where $K = k_P$ is the proportional feedback gain. For the external active coils, the above feedback logic, together with the wall jump condition, Eq. (4), helps to relate the coefficient c to ψ_f for different types of sensors. For the internal active coils, similar relations of the coefficients c_1 and c_2 to ψ_f are obtained by employing the above feedback logic with condition $r\psi'/\psi|_{r_w+} = -m$ and the wall jump condition (4) on the perturbed field in the vacuum region $r_f < r < r_w$. This allows us to calculate the logarithmic derivative of the perturbed flux function just outside the plasma surface

$$\left.\frac{r\psi'}{\psi}\right|_{a+} = m\left[1 - \frac{2}{1 - \alpha_P a^{2m}/r_w^{2m}}\right], \tag{7}$$

where α_P is a key quantity describing different configurations of the proportional feedback system

$$\alpha_P = \begin{cases} \dfrac{\gamma\tau_w + 2mk_P}{\gamma\tau_w + 2mk_P + 2m} & ext.coil + rad.sensor, \\[2ex] \dfrac{(1-2mk_P)\gamma\tau_w + 2m^2 k_P}{(1-2mk_P)\gamma\tau_w + 2m - 2m^2 k_P} & ext.coil + ext.pol.sensor, \\[2ex] \dfrac{\gamma\tau_w + 2m^2 k_P}{\gamma\tau_w + 2m - 2m^2 k_P} & ext.coil + int.pol.sensor, \\[2ex] \dfrac{\gamma\tau_w + 2mk_P\alpha_f}{\gamma\tau_w + 2mk_P + 2m} & int.coil + rad.sensor, \\[2ex] \dfrac{\gamma\tau_w + 2m^2 k_P\alpha_f}{\gamma\tau_w + 2m + 2m^2 k_P} & int.coil + ext.pol.sensor, \\[2ex] \dfrac{(1+2mk_P\alpha_f)\gamma\tau_w + 2m^2 k_P\alpha_f}{(1+2mk_P)\gamma\tau_w + 2m + 2m^2 k_P} & int.coil + int.pol.sensor. \end{cases}$$

Connecting Eqs. (2), (3), and (7) via relation (5) across various regions, we derive the following expression for Δ'_{ext} at the rational surface r_s in the presence of proportional feedback control:

$$\Delta'_{ext,P}(K,\gamma) = -\frac{2m}{r_s}\left[\frac{B_P}{\alpha_s + (1-\alpha_s)B_P} - \frac{A}{\alpha_0 + (1-\alpha_0)A}\right], \quad (8)$$

where $B_P = \frac{1}{1-\alpha_w\alpha_P} - \hat{\beta}$. Comparing the close-loop expression (8) with the open-loop expression (6), we find that feedback modifies the external tearing index only via the B_P factor. The proportional feedback gain K enters Eq. (8) via the α_P factor. The change of Δ'_{ext} due proportional feedback is

$$\delta\Delta'_P = \Delta'_{ext,P}(K,\gamma) - \Delta'_{ext}(K=0,\gamma)$$
$$= -\frac{2m}{r_s}\frac{(\alpha_P - \alpha_{rw})\alpha_s\alpha_w}{[C+(1-\alpha_s-C)\alpha_w\alpha_P][C+(1-\alpha_s-C)\alpha_w\alpha_{rw}]}, \quad (9)$$

where $C = \alpha_s + (1-\alpha_s)(1-\hat{\beta})$. We remark that the above result assumes the same growth rate between the open-loop and close-loop systems, which is generally not the case. The growth rate needs to be self-consistently evaluated based on the RWM dispersion relations (with or without feedback). This will be addressed in Secs. III–V.

C. Close-loop with proportional–derivative feedback

Now we consider proportional–derivative (PD) feedback with the control logic of $\psi_f = -[k_P + sk_D]y$, where k_D is the derivative gain and s is the eigenvalue of the close-loop system. Following a similar procedure to that outlined for the P-controller, we arrive at the following expression for the external tearing index in the presence of PD-feedback:

$$\Delta'_{ext,PD}(K,\gamma) = -\frac{2m}{r_s}\left[\frac{B_{PD}}{\alpha_s + (1-\alpha_s)B_{PD}} - \frac{A}{\alpha_0 + (1-\alpha_0)A}\right], \quad (10)$$

where $B_{PD} = \frac{1}{1-\alpha_w\alpha_{PD}} - \hat{\beta}$ and

$$\alpha_{PD} = \begin{cases} \dfrac{\gamma\tau_w(1+2mk_D)+2mk_P}{\gamma\tau_w(1+2mk_D)+2mk_P+2m} & ext.coil + rad.sensor, \\[3mm] \dfrac{\gamma\tau_w(1-2mk_P+2m^2k_D)+2m^2k_P-2mk_D(\gamma\tau_w)^2}{\gamma\tau_w(1-2mk_P-2m^2k_D)+2m-2m^2k_P-2mk_D(\gamma\tau_w)^2} & ext.coil + ext.pol.sensor, \\[3mm] \dfrac{\gamma\tau_w(1+2m^2k_D)+2m^2k_P}{\gamma\tau_w(1-2m^2k_D)-2m^2k_P+2m} & ext.coil + int.pol.sensor, \\[3mm] \dfrac{\gamma\tau_w(1+k_D\alpha_f)+2mk_P\alpha_f}{\gamma\tau_w(1+2mk_D)+2mk_P+2m} & int.coil + rad.sensor, \\[3mm] \dfrac{\gamma\tau_w(1+2m^2k_D\alpha_f)+2m^2k_P\alpha_f}{\gamma\tau_w(1+2m^2k_D)+2m^2k_P+2m} & int.coil + ext.pol.sensor, \\[3mm] \dfrac{\gamma\tau_w(1+2mk_P\alpha_f+2m^2k_D\alpha_f)+2m^2k_P\alpha_f+2mk_D\alpha_f(\gamma\tau_w)^2}{\gamma\tau_w(1+2mk_P+2m^2k_D)+2m+2m^2k_P+2mk_D(\gamma\tau_w)^2} & int.coil + int.pol.sensor. \end{cases}$$

The change of Δ'_{ext}, due to PD-control, becomes

$$\delta\Delta'_{PD} = \Delta'_{ext,PD}(K,\gamma) - \Delta'_{ext}(K=0,\gamma)$$
$$= -\frac{2m}{r_s}\frac{(\alpha_{PD} - \alpha_{rw})\alpha_s\alpha_w}{[C+(1-\alpha_s-C)\alpha_w\alpha_{PD}][C+(1-\alpha_s-C)\alpha_w\alpha_{rw}]}, \quad (11)$$

where the constant C is the same as that from Eq. (9).

D. Inner layer solutions

Expressions (6), (8), and (10) depend on the mode eigenvalue γ, which is *a priori* unknown. The only case, where the value of Δ'_{ext} can be explicitly calculated, is when the wall time vanishes (i.e., in the absence of the resistive wall). This was the case considered in Ref. 34. In more general cases, we need to solve the dispersion relation for the RWM by setting the external tearing index to zero (for the IP-RWM)

or by matching the external and internal solutions (for the RP-RWM) in order to find the mode eigenvalue γ.

For a pressureless plasma (i.e., $\beta = 0$) without the GGJ effect, the inner tearing index at the resonant surface is conveniently written as[35]

$$\Delta'_{int}(\gamma) = 2.12(ns)^{-1/2}S^{3/4}(\gamma\tau_A)^{5/4}, \quad (12)$$

where s is the magnetic shear (at the mode rational surface) and S is the Lundquist number. For a plasma with finite equilibrium pressure (and pressure gradient) at the rational surface, it is helpful to consider the GGJ effect. The inner tearing index in this case takes the form[36,37]

$$\Delta'_{int}(\gamma) = 2.12A_s(\gamma\tau_A)^{5/4}\left[1 - \frac{\pi}{4}D_RB_s(\gamma\tau_A)^{-3/2}\right], \quad (13)$$

where $A_s = (ns)^{-1/2}(1+2q_{r_s}^2)^{1/4}S^{3/4}$ and $B_s = (ns)(1+2q_{r_s}^2)^{-1/2}S^{-1/2}$. D_R is the resistive interchange index, which is roughly proportional to the plasma pressure at the rational surface. Note that D_R is typically a

small negative number for tokamak plasmas, which we shall treat as a free parameter in our analytic model. We emphasize that, for a given plasma equilibrium, the D_R value is fixed. Therefore, treating D_R as a free parameter introduces in-consistency in the model, which on the other hand has minor consequences on our main conclusions reported later on. Treating D_R as a free parameter allows us to examine the effect of the strength of the GGJ effect on the RP-RWM. We also note this *ad hoc* inclusion of the GGJ physics into the inner layer is not consistent with the equilibrium profiles that we choose. For an equilibrium with generic current and pressure profiles, the external tearing index can only be numerically calculated.

Knowing the analytic forms for both the inner and outer tearing indices, the matching condition

$$\Delta'_{\text{ext}}(K, \gamma) = \Delta'_{\text{int}}(\gamma) \tag{14}$$

then leads to the dispersion relation for the RP-RWM in the presence of magnetic feedback. As another remark here, we mention that the effect of the plasma rotation can also be included into the matching approach by adding a Doppler shift (associated with plasma rotation) to the mode eigenvalue when evaluating the inner tearing index (12) or (13). The outer tearing index remains unchanged since we assume that a slow (subsonic) flow does not affect the outer region solution. Plasma rotation has been found to shrink the stable domain near the marginal stability curve.[23] In this work, however, we shall neglect the plasma flow effect.

Since the above dispersion relation involves the eigenvalue γ in a non-linear manner, we shall provide numerical solutions in Secs. III–V. We then insert the calculated γ value into the external tearing index in order to find out how the magnetic feedback modifies the tearing index. We perform the study for the IP-RWM (Sec. III), RP-RWM (Sec. IV), and RP-EK (Sec. V), respectively. For each type of instability, we shall consider a proportional control scheme while varying feedback coil configurations by utilizing Eq. (8). Additional study of the effect of the derivative feedback gain is reported in Appendix C. In this study, we neglect the integral control action which mainly shapes the control performance (e.g., reduces the settling time). We leave tearing index modification by more advanced controllers to future studies.

III. FEEDBACK CONTROL OF IP-RWM

Analytic theory of active control of the IP-RWM has been well developed during past years. The previous study, however, largely relied on directly solving the coupled MHD-feedback equations[38,39] or on the PRM.[28–30] We follow a different approach here, namely, by requiring vanishing tearing index at the resonant surface for the IP-RWM. We shall show that both the PRM approach and the matching approach yield the same feedback results.

We consider two plasma equilibria, one with vanishing plasma pressure ($\beta = 0$) and one with a finite equilibrium pressure ($\beta = 0.03$). Chosen are the following basic parameters: $a = 1$, $m = 2$, $n = 1$, $r_0 = 0.63a$, and $r_w = 1.2a$. Furthermore, we assume $r_f = 1.3a$ for the external active coil and $r_f = 1.1a$ for the internal active coil. For the resistive wall, the wall time is fixed at $\tau_w = 10^4 \tau_A$. The value of the on-axis safety factor q_0 will be varied to ensure a typical RWM regime.

Indeed, the open-loop stability can be tuned by scanning q_0. One example with $\beta = 0$ is shown in Fig. 2(a), where we show the mode

growth rate with the resistive wall and also compare with that in the ideal-wall limit. The growth rate here is obtained by solving the dispersion relation $\Delta'_{\text{ext}} = 0$ for the ideal plasma and Eq. (14) for the resistive plasma, but at feedback gain $K = 0$. Note that the inertial term, associated with the A_1 factor [cf. expression (6)], has been retained in solving the aforementioned dispersion relations. It is important to include this inertial factor in order to recover the ideal-plasma external kink (IP-EK) and the RP-EK regimes shown in Fig. 2(a). Transition from the RWM regime to the EK regime occurs at $q_0 = 1.076$ [indicated by the vertical dashed line in Fig. 2(a)]. In the ideal-wall limit, both the IP-RWM and the RP-RWM branches become stable when $q_0 < 1.076$. We emphasize that, with our parameter setting, the threshold value of $q_0 = 1.076$ is the solution of $1 - (m - nq_0) - (r_0/r_w)^{2m} = 0$ (Appendix A). The EK regime corresponds to $1 - (m - nq_0) - (r_0/r_w)^{2m} > 0$ at $q_0 > 1.076$, and the RWM regime corresponds to $1 - (m - nq_0) - (r_0/r_w)^{2m} < 0$ at $q_0 < 1.076$. At $q_0 > 1.076$, the EK is unstable with the ideal wall. The aforementioned inertial term is negligible for the RWM regime.

We note that Ref. 22 found that the resistive instability cannot be feedback stabilized when the condition $\zeta_0 > -\Delta_1$ is satisfied. In our notations and with a step-function equilibrium current density, it is straightforwardly shown that $\zeta_0 = 2m/[r_0(m - nq_0)]$ and $-\Delta_1 = 2m\alpha_0/[r_0(\alpha_0 - 1)]$, where α_0 is defined in Eq. (6). The above condition from Ref. 22 is thus equivalent to $\alpha_0 + (1 - \alpha_0)A > 0$ in our notations. This condition is satisfied only if q_0 exceeds two, or in other words, when there is no resonant surface anymore within the plasma for the considered $m/n = 2/1$ resistive instability. Note also that the RP-EK instability that we consider in this work (at $q_0 = 1.2$) does not satisfy the above quoted condition.

Inclusion of the plasma resistivity is found to substantially reduce the growth rate of the RWM (as well as that of the EK to large extent). This agrees with our previous finding[13,14] although the latter was obtained via a completely different approach (i.e., the extended energy principle approach for the open-loop RWM). The relatively small growth rate for the three instabilities, i.e., the IP-RWM, RP-RWM, and RP-EK, implies that active magnetic control (with practically reasonable control response time) can be applied to stabilize these modes. This is precisely the subject of the following studies. At fixed q_0, finite equilibrium pressure modifies the mode growth rate for the IP-RWM [Fig. 2(b)] as well as for the RP-RWM and the RP-EK [Fig. 2(c)]. The growth rate of the instabilities generally increases with β. An exception is the sharp transition near $\beta = 0$ in Fig. 2(c). This is associated with the Pfirsch–Shlutter inertia enhancement (and the lack thereof at $\beta = 0$) at finite plasma pressure. The strong destabilization of the open-loop growth rate for the IP-RWM is largely due to the pressure drive on the external tearing index.[40] The smooth variation of the mode instability allows us to choose representative β values for later studies, specifically $\beta = 0$ and $\beta = 0.03$ for the RWM and $\beta = 0.05$ for the RP-EK. We mention that more systematic analytic study of the beta effect on the open-loop RP-RWM stability has been made in Ref. 41, assuming a layer model without the GGJ-physics.

As a final remark here, we discuss the open-loop and close-loop stability of the case without a wall. The open-loop growth rates of the no-wall IP-EK and RP-EK are plotted in Fig. 2(a) as well, showing that the growth rate of the IP-EK is large and almost independent of q_0. Inclusion of the plasma resistivity substantially reduces the mode growth rate even in the absence of a wall. For our equilibrium, the
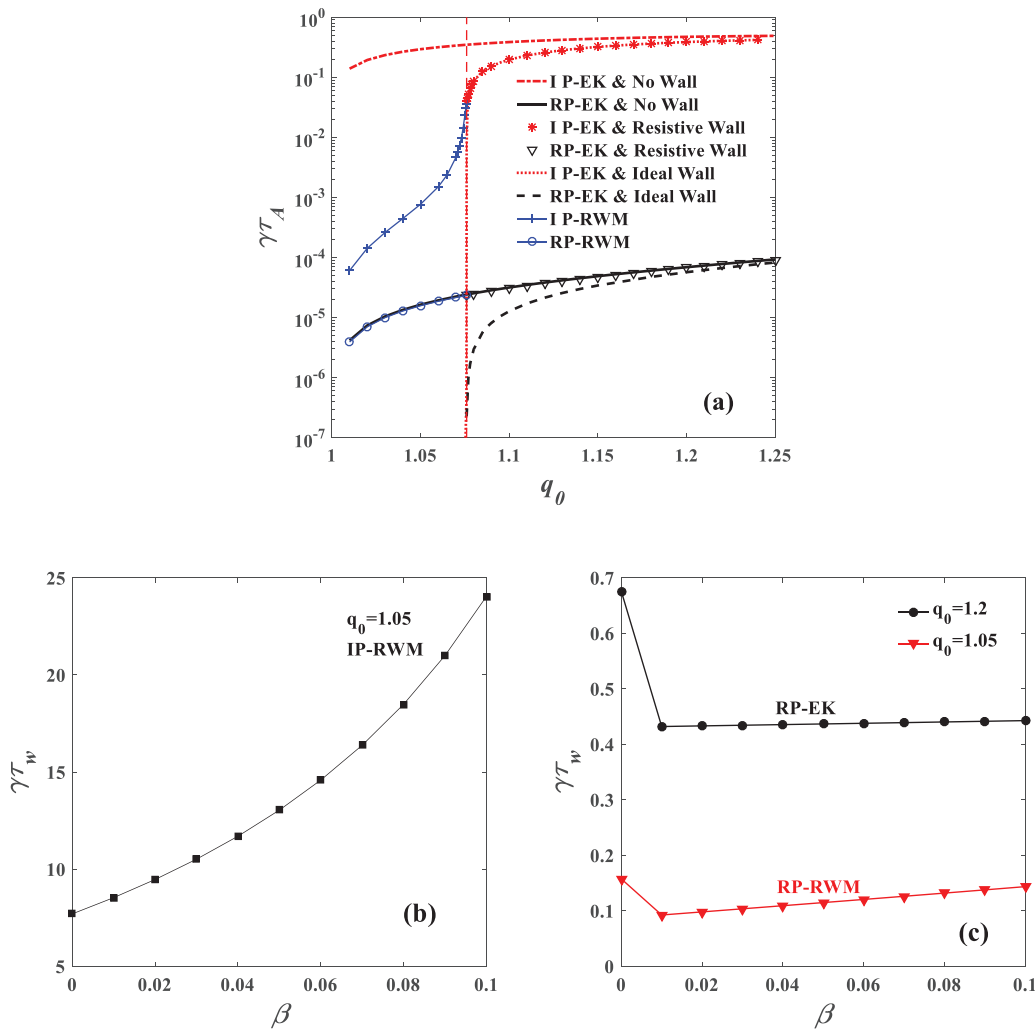
FIG. 2. The (a) open-loop growth rate of the $n = 1$ instability in different regimes, without equilibrium pressure $\beta = 0$, while scanning the on-axis safety factor q_0: the ideal plasma external kink (IP-EK) and the resistive plasma external kink (RP-EK), the ideal plasma resistive wall mode (IP-RWM), and the resistive plasma resistive wall mode (RP-RWM). The vertical dashed line indicates the transition value ($q_0 = 1.076$) from the RWM regime to the EK regime. The dashes-dotted line, star-points, and dotted line represent the growth rates of the IP-EK without wall ($\tau_w = 0$), with the resistive wall ($\tau_w = 10^4$), and with the ideal wall, respectively. The solid line, inverted-triangle points, and dashed line represent the growth rates of the RP-EK without wall, with the resistive wall, and with the ideal wall, respectively. Note that the growth grate of the mode in the resistive plasma nearly overlaps between the no-wall and the resistive wall cases. Shown in (b) is the open-loop growth rate of the IP-RWM with increasing β at fixed $q_0 = 1.05$. Shown in (c) is the open-loop growth rate of the RP-RWM (at $q_0 = 1.05$) and the RP-EK (at $q_0 = 1.2$) while scanning the equilibrium pressure. For the resistive plasma instabilities, the plasma resistivity is fixed $\eta = 2 \times 10^{-8}$.

growth rate of the no-wall RP-EK is close to that of the RP-EK with the resistive wall. We point out that the difference between the no-wall and resistive-wall cases here depends on the ratio of the plasma resistivity to the wall resistivity. For instance, the difference becomes more pronounced with increasing the wall time at fixed plasma resistivity. In terms of the close-loop stability, magnetic feedback cannot stabilize the no-wall IP-EK but can significantly reduce the external tearing index for the RP-EK, as shown in Ref. 34.

Now we numerically solve the close-loop dispersion relation $\Delta'_{\text{ext, P}}(K, \gamma) = 0$ [i.e., expression (8) = 0] in the presence of a P-controller. The results are plotted in Fig. 3 while scanning the

proportional feedback gain $K = k_P$. Compared are the growth rates of the IP-RWM in a plasma with vanishing equilibrium pressure $\beta = 0$ [Fig. 3(a)] and with finite equilibrium pressure $\beta = 0.03$ [Fig. 3(b)]. Six combinations of the active and sensor coil types are considered as indicated in the figure.

Proportional feedback can stabilize the IP-RWM, either with or without pressure, when the proportional gain reaches a certain critical value. This holds for all six feedback coil configurations. The stabilizing effect with internal active coils is stronger than that with external active coils at small feedback gain, independent of the choice of the sensor type (but assuming the same sensor type). At large gain
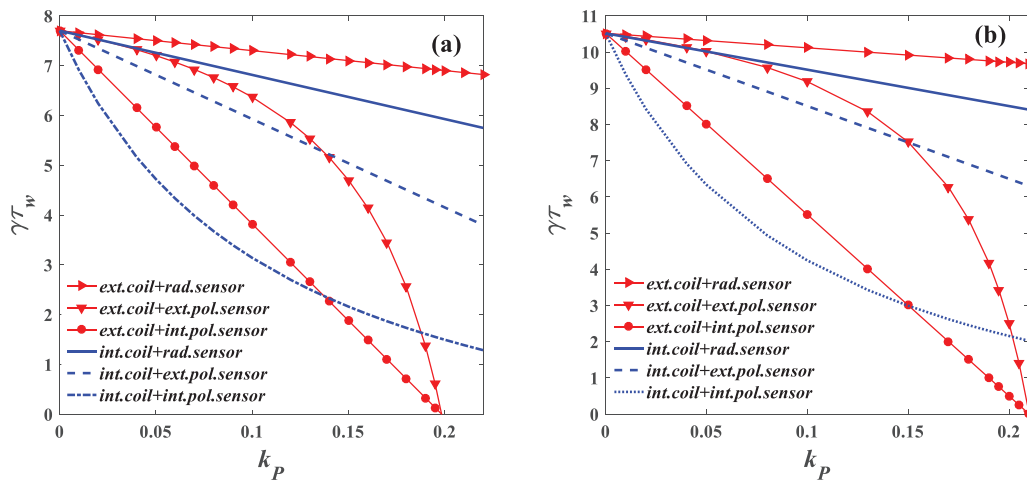
FIG. 3. The growth rate of the $n = 1$ IP-RWM vs the proportional feedback gain value k_P, assuming various combinations of the active and sensor coil types and (a) vanishing equilibrium pressure $\beta = 0$ and (b) finite equilibrium pressure $\beta = 0.03$. The on-axis safety factor is fixed at $q_0 = 1.05$.

values and with (either internal or external) poloidal sensors, however, feedback with external active coils outperforms that with internal active coils. In fact, we find similar results also for RP-RWM and RP-EK as will be reported later on.

The above finding appears to be counter-intuitive. The expectation is that, with the same type of sensor coils, placing the active coils inside the resistive wall should always be better than placing them outside the wall for two reasons. First, the control field is stronger since the internal active coil is closer to the plasma. Second, with the internal active coils, the control field does not need to penetrate through the resistive wall in order to reach the plasma. We remark that the second argument does not apply to the case of marginal stability (assuming that the marginal stability is reached at vanishing mode frequency) since the wall eddy current vanishes in this case. But the first argument always applies.

It turns out that this counter-intuitive behavior is the result of the single harmonic approximation that we adopt in this study. The single harmonic approximation is a natural choice for the matching approach (as well as for the cylindrical plasma). Note that the equilibrium that we choose has only a single resonant harmonic $m/n = 2/1$. The multi-harmonic coupling effect thus can only come from the non-resonant harmonics and is a feedback coil geometry effect.

To illustrate this, we return to the PRM approach (Appendix B). The latter allows us to include multiple poloidal harmonics into the plasma response transfer function despite the fact that the 2/1 mode is the only unstable mode in the spectrum. Inclusion of multiple poloidal harmonics is needed primarily to properly describe the feedback coil geometry,[28] which is where our intuition develops from. In other words, window-pane active coils and point-wise poloidal sensor signals require many poloidal harmonics to resolve. As soon as we add all the other (non-resonant) harmonics (associated with stable RWM) into the PRM, we find that the internal active coils always outperform the external counterpart [Fig. 12(c), Appendix B].

Even more interestingly, it turns out that the major role in resolving the puzzle is played by the $m = -2$ harmonic. By only including the $m = \pm 2$ contributions into the PRM, the

aforementioned counter-intuitive phenomenon also disappears [Fig. 12(b), Appendix B]. The fundamental reason here is a cancelation effect between the $+m$ and $-m$ harmonics as discovered in Ref. 30.

As mentioned before, it is unfortunately not straightforward to include multiple harmonics (in particular that of the non-resonant sideband) into the matching approach. (The PRM approach as developed in Refs. 29–31 is suitable for including multiple harmonics but is not suitable for including the resistive layer physics.) Therefore, caution needs to be taken when discussing the feedback results (in particular that with the external active coils and poloidal sensors) predicted by the matching approach with single harmonic approximation, which does not properly describe the realistic feedback coil geometry as adopted in experiments.

As a final remark to the results shown in Fig. 3, we notice that the open-loop growth rate increases with equilibrium pressure, as shown in Fig. 2(b). The critical gain required for full stabilization of the IP-RWM is larger [$\beta = 0.03$, Fig. 3(b)].

## IV. FEEDBACK CONTROL OF RP-RWM VIA MODIFICATION OF Δ'_{ext}

If the IP-RWM feedback study presented in Sec. III can be carried out with either the PRM or matching approach, the latter is much more suitable for studying feedback control of the RP-RWM. Even more interestingly, the matching approach allows us to quantify the effect of magnetic feedback on the tearing index Δ'_{ext}. In what follows, we demonstrate that feedback indeed modifies Δ'_{ext}. Moreover, we show that feedback modification of the external tearing index does not depend on the inner layer physics, i.e., on variation of the D_R value. The basic plasma parameters (except those in the resistive layer) are assumed the same as that from Sec. III.

With proportional control, stability of the close-loop for the RP-RWM is determined by solving the dispersion relation (14) which links Eq. (8) with Eq. (12) or (13), depending on whether the GGJ effect is included into the layer model. As mentioned before, we include the GGJ physics [Eq. (13)] into the inner layer for the equilibrium with finite pressure. The feedback results for both equilibria

(with vanishing or finite pressure) are summarized in Fig. 4. Similar to results reported in Sec. III for the IP-RWM, proportional feedback reduces the growth rate of the RP-RWM, with all six feedback coil configurations considered in this work. The combination of internal active coils with internal poloidal sensor performs the best at low feedback gain. At higher feedback gain, we again obtain the counter-intuitive result of the superior performance by the external active coils. Since the behavior is qualitatively similar to that of the IP-RWM, we expect that the same reasoning (i.e., the single harmonic approximation vs the requirement of multiple poloidal harmonics to correctly describe the feedback coil geometry) also applies here to explain this counter-intuitive behavior.
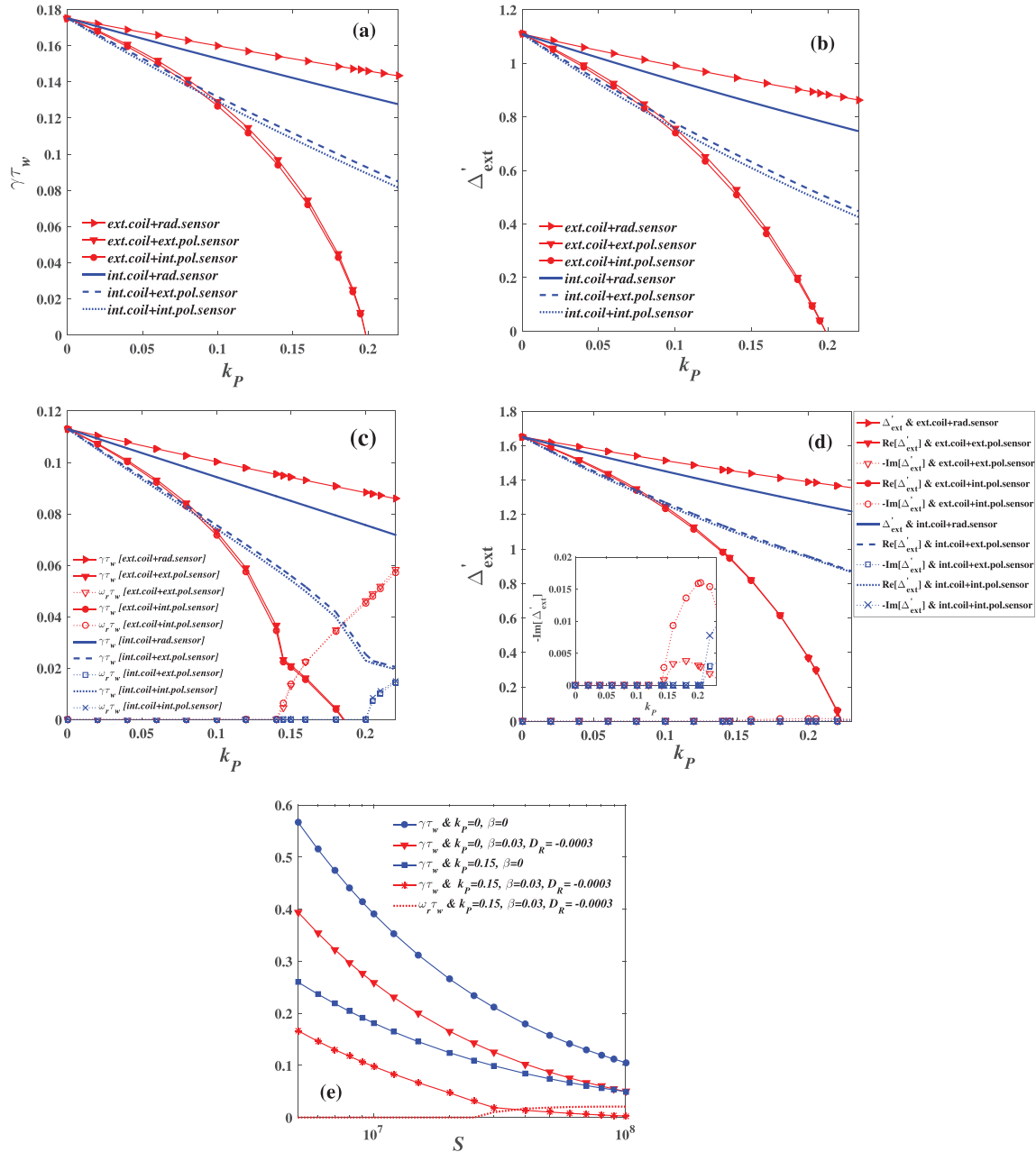
FIG. 4. Close-loop results for the $n = 1$ RP-RWM, assuming equilibria with [(a) and (b)] vanishing pressure $\beta = 0$ and [(c) and (d)] finite pressure $\beta = 0.03$ with the GGJ included into the inner layer tearing index ($D_R = -0.0003$). Compared are results with various feedback coil configurations assuming proportional control. Plotted are [(a) and (c)] the mode growth rate and [(b) and (d)] the external tearing index. Shown in (e) are the open-loop and close-loop growth rates for the RP-RWM while scanning the Lundquist number S, assuming a combination of external active coils with the internal poloidal sensor. The on-axis safety factor is fixed at $q_0 = 1.05$.

We now analyze some details of the results presented in Fig. 4, first focusing on the vanishing equilibrium pressure case without the GGJ effect. Figure 4(a) shows that the critical gain values for k_P, corresponding to marginal stability of the RP-RWM with the external active coils and the internal or external poloidal sensors, coincide. This is because the wall eddy current disappears at the marginal instability. Therefore, the wall is effectively in absence under this peculiar circumstance. In other words, the (normally qualitative) difference between the internal and external poloidal sensors disappears at the marginal instability point (and with vanishing mode frequency which is the case here).

Inserting the mode growth rate shown in Fig. 4(a) back into expression (8), we obtain feedback modification of the external tearing index as reported in Fig. 4(b). The overall behavior, among various combinations of the feedback coils, resembles that of the stability plot shown in Fig. 4(a). This is understandable since the inner tearing index in this case scales with the mode growth rate in a simple proportionality manner [Eq. (12)]. Nevertheless, Fig. 4(b) convincingly demonstrates that feedback reduces the external tearing index, and, by doing so, it stabilizes the RP-RWM.

Next, we discuss Figs. 4(c) and 4(d) for the finite pressure equilibrium case, where the GGJ effect is included into the inner layer tearing index [Eq. (13)]. The feedback results are generally similar to that without the GGJ-effect [Figs. 4(a) and 4(b)]. One qualitative difference though is the appearance of complex eigenvalues (i.e., finite mode frequencies) at large proportional gains as shown in Fig. 4(c). This occurs for the close-loop with either internal or external poloidal sensors. It is known that, in the absence of feedback, the GGJ effect can introduce complex frequency to the RP-RWM even for a static equilibrium if the D_R value is sufficiently negative.[14] In our case, however, the D_R value is chosen such that the open-loop eigenvalue is real. The finite mode frequency is thus introduced by the feedback action (but in the presence of the GGJ effect).

Figure 4(d) shows the corresponding Δ'_{ext} for the case with GGJ effect. The general trend of the proportional feedback is again to reduce Δ'_{ext}. The most interesting observation here, however, is that the corresponding external tearing index becomes complex-valued at sufficiently large feedback gain. The imaginary part of Δ'_{ext} is small (by about three orders of magnitude in this case) compared to that of the real part, but much larger imaginary part is also obtained as will be shown in later examples. Note that complex Δ'_{ext} occurs whenever the close-loop eigenvalue becomes complex. This feature of complex Δ'_{ext} is qualitatively different from the open-loop TM theory, where sufficiently large GGJ effect introduces finite mode frequency but the tearing index remains real-valued.

Close examination of the close-loop external tearing index reveals two possible perturbed energy sources from the outer region that can introduce complex Δ'_{ext} in the presence of a rotating close-loop RP-RWM (in the static plasma). One is the plasma inertia, while the other is the presence of a resistive wall. For the RWM, the plasma inertia (from the outer region) is known to play a minor role on the mode dynamics. In fact, in our example, the inertia term [associated with the A_1 factor, see Eq. (6)] is about $(\tau_w/\tau_A)^2 = 10^8$ times smaller than that due to the resistive wall, with the latter providing an order unity contribution to Δ'_{ext}. The major role in inducing complex-valued external tearing index is thus played by the resistive wall, which provides perturbed energy dissipation due to the wall eddy current. To further

verify this conclusion, we performed feedback calculations similar to that presented in Figs. 4(c) and 4(d), but this time assuming $\tau_w = 0$ in Eq. (8). The close-loop Δ'_{ext} indeed becomes real-valued in this case even in the presence of large feedback gain and complex RP-RWM eigenvalues.

The results shown in Figs. 4(a)–4(d) assume a fixed Lundquist number of $S = 5 \times 10^7$. The feedback results remain qualitatively similar with different choices of the Lundquist number. Figure 4(e) compares the open-loop and close-loop instabilities while scanning the Lundquist number at fixed proportional feedback gain. Considered is a feedback configuration with external active coils and the internal poloidal sensor. Increasing the Lundquist number reduces the mode instability for both the open-loop and close-loop systems, with the open-loop result being consistent with that reported in Ref. 13.

Another interesting observation is that the real part of the external tearing index is nearly independent of the assumed D_R value when we scan the feedback gain despite the fact that the close-loop eigenvalue substantially varies with D_R. This is illustrated in Fig. 5, where we assume a control scheme with external active coils and the internal poloidal sensor. For a given D_R value, the close-loop eigenvalue becomes complex at certain feedback gain, but the mode is still unstable [Fig. 5(a)]. Further increasing feedback gain results in full stabilization of the RP-RWM, with the critical gain value (for marginal stability) increasing with increasing the amplitude of D_R. A small imaginary part [inset in Fig. 5(b)] of Δ'_{ext} again appears when the close-loop eigenvalue becomes complex. But the real part of Δ'_{ext} is almost independent of the choice for the D_R value. In other words, the results show that the magnetic feedback system modifies the external tearing index almost independent of the inner layer physics.

V. FEEDBACK CONTROL OF RP-EK VIA MODIFICATION OF Δ'_{ext}

As the final step of investigation, we consider feedback stabilization of the RP-EK. Active control of the EK is normally not practically feasible due to the fast open-loop growth (in Alfvenic timescale). This is, however, not the case for the RP-EK due to substantial reduction of the mode growth rate by the plasma resistivity, as shown in Fig. 2. We shall again consider P-control with or without the GGJ physics in the inner layer. The basic plasma parameters remain the same as that in Sec. III, except for the on-axis safety factor $q_0 = 1.2$ and the equilibrium pressure $\beta = 0.05$. The Lundquist number is fixed at $S = 5 \times 10^7$. As mentioned before, these choices merely represent typical values. Our final conclusions are not sensitive to these choices. We remark that, at $q_0 = 1.2$, a new rational surface ($q = 3$) appears inside the plasma ($q_a = 3.0234$). With our parameter settings, the $m = 3$ mode is stable and is thus not studied here.

The difference from the RP-RWM study is that the plasma inertia is still retained in evaluating the external tearing index. We note that the plasma inertia is critical for the EK as soon as the mode growth rate is large. (It can be easily verified that, without including the inertial term, the IP-EK becomes stable when $q_0 < 1.076$ with our equilibrium model, leading to un-physical results.) On the other hand, when the EK instability is significantly weakened by the plasma resistivity (i.e., the RP-EK), the inertial effect again becomes less important. We nevertheless keep the plasma inertia in the following study for consistency, so that the IP-EK regime can be recovered at vanishing plasma resistivity.
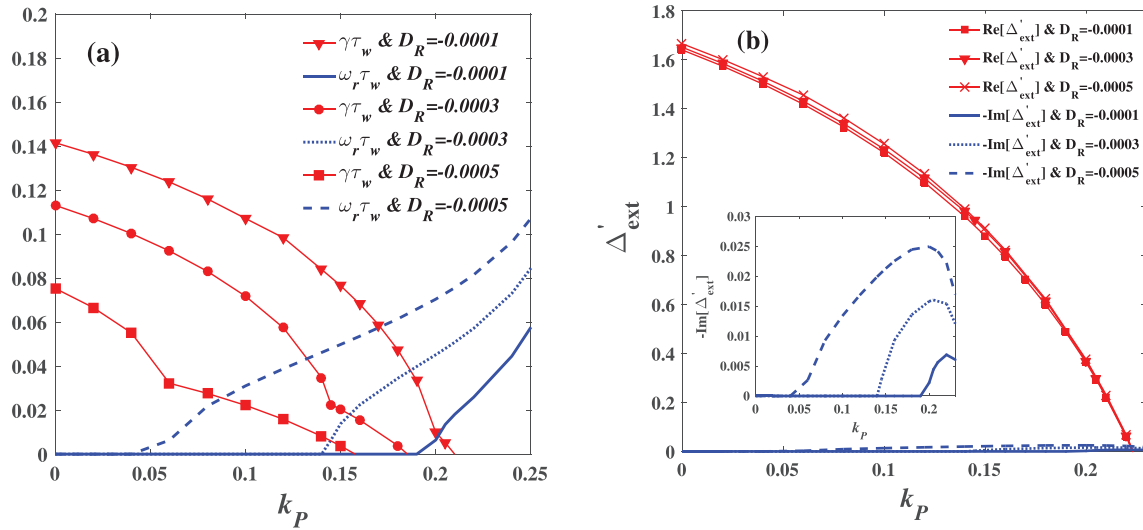
FIG. 5. Close-loop results for the $n = 1$ RP-RWM for (a) the mode eigenvalues and (b) the external tearing index while scanning the proportional feedback gain and varying the value of the resistive interchange index. Considered is a plasma with finite equilibrium pressure ($\beta = 0.03$). Assumed is a control scheme with the external active coil and the internal poloidal sensor. The on-axis safety factor is fixed at $q_0 = 1.05$.
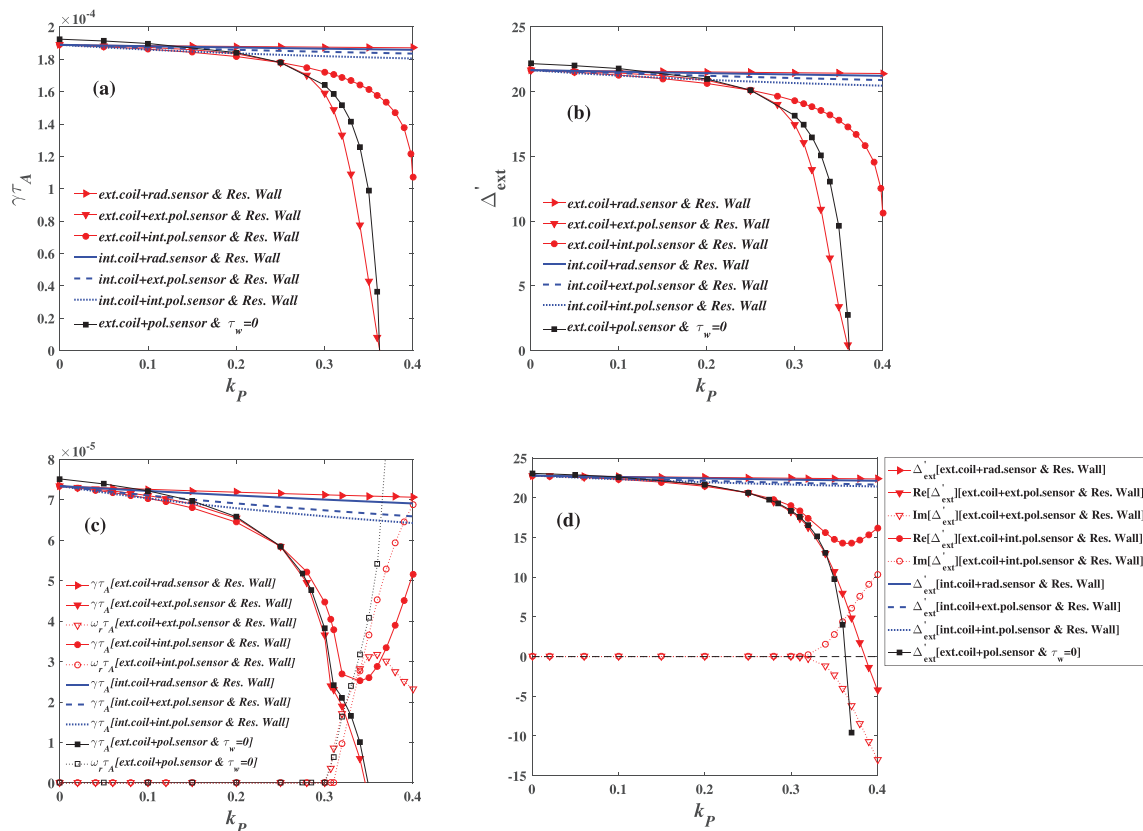

FIG. 6. Close-loop results for the $n = 1$ RP-EK with ($\tau_w = 10^4 \tau_A$) and without ($\tau_w = 0$) resistive wall, assuming equilibria with [(a) and (b)] vanishing pressure $\beta = 0$ and [(c) and (d)] finite pressure $\beta = 0.05$ with the GGJ included into the inner layer tearing index ($D_R = -0.01$). Compared are results with various feedback coil configurations assuming proportional control. Plotted are [(a) and (c)] the mode growth rate and [(b) and (d)] the external tearing index. The on-axis safety factor is fixed at $q_0 = 1.2$.

Figure 6 shows that feedback stabilization of the RP-EK is generally weak due to weak modification of the external tearing index. The exception is the coil combination with external active coils and the internal or external poloidal sensor. However, as pointed out in Sec. III, the strong stabilization with external active coils should be viewed with caution due to the artifact associated with the single harmonic approximation. Another observation is the large difference in the feedback results between the internal and external poloidal sensors. This is due to much stronger instability (the open-loop growth rate of the RP-EK which is about one order of magnitude higher than that of the RP-RWM); it induces larger eddy currents in the resistive wall.

With external active coils, the two stability curves with internal and external poloidal sensors intersect at the feedback gain value of $k_P = 0.25$. This is not a co-incidence. Detailed analysis of the

expression (8) for the external tearing index reveals that, at this gain value, or more generally at $k_P = 1/2m$, the parameter $\alpha_P = 1$ holds independent of the wall time, resulting in the same stabilization effect.

Similar to the RP-RWM, inclusion of the GGJ effect results in a rotating RP-EK at large proportional gain ($k_P > 0.3$) and with external active coils [Fig. 6(c)]. The corresponding external tearing index also becomes complex-valued, with large magnitude of $\mathrm{Im}(\Delta'_{ext})$ in this case. The imaginary part of the outer tearing index is again primarily introduced by the wall eddy current induced perturbed energy dissipation.

To further illustrate the last point, we report the feedback results for the RP-EK in the limit of $\tau_w = 0$ in Fig. 7. Note that, by definition, we are considering here an RP-EK (not RP-RWM) instability here despite that $q_0 < 1.076$ since $\tau_w = 0$. The results show that the
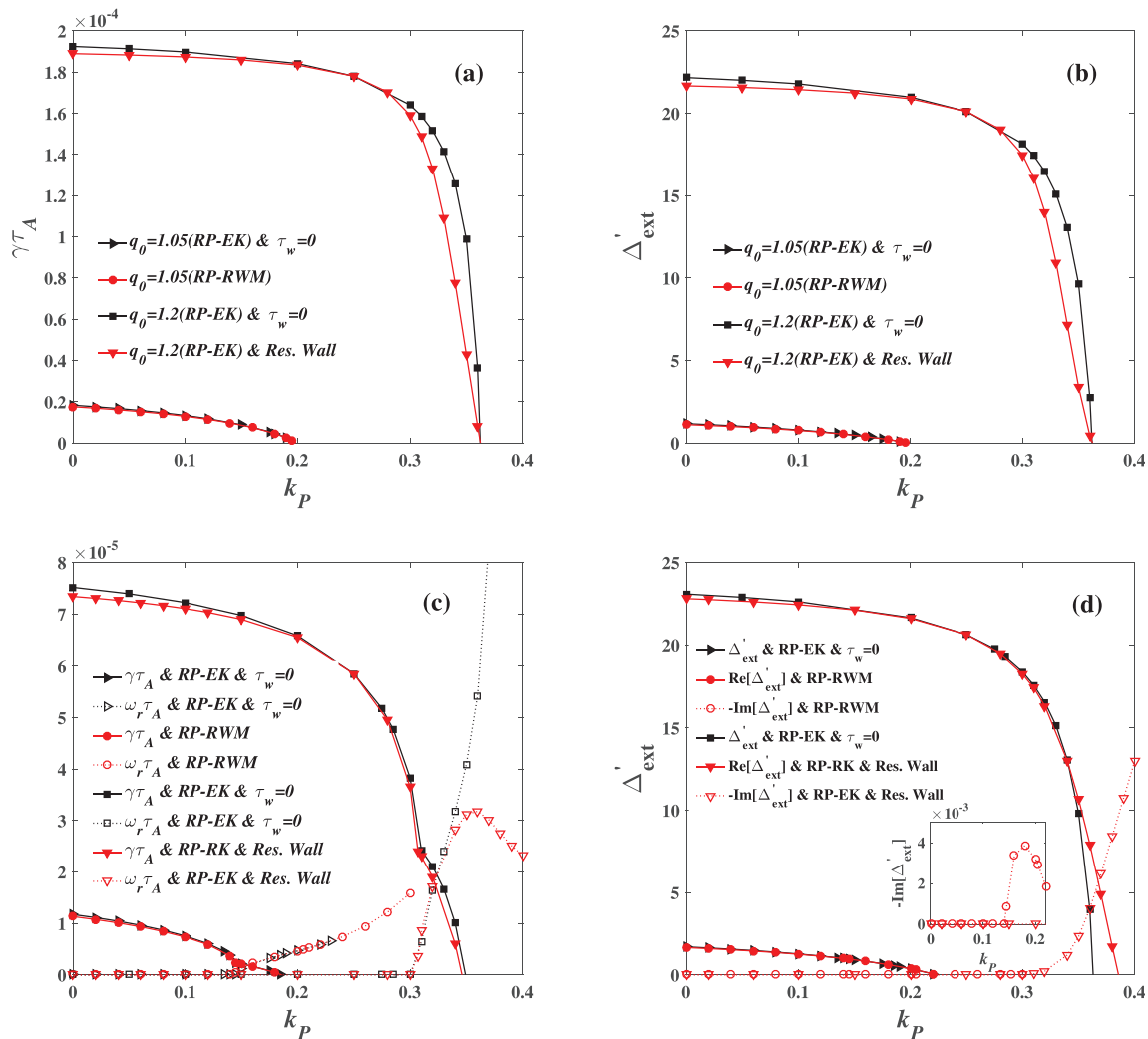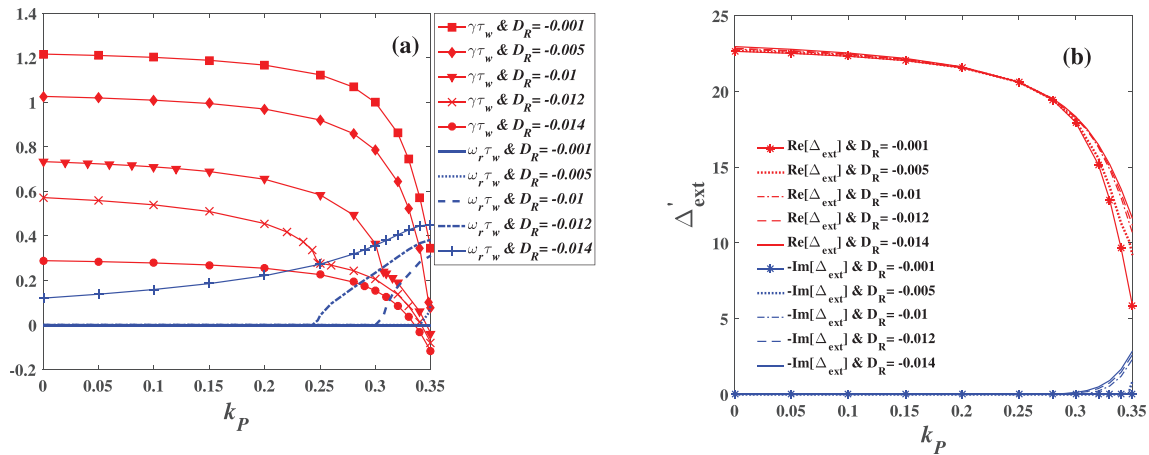

FIG. 7. Close-loop results for the $n = 1$ RP-RWM ($q_0 = 1.05$) and RP-EK ($q_0 = 1.2$), assuming equilibria with [(a) and (b)] vanishing pressure and [(c) and (d)] finite pressure with the GGJ included into the inner layer tearing index ($\beta = 0.03$ for RP-RWM and $\beta = 0.05$ for RP-EK). Compared are results with ($\tau_w = 10^4\tau_A$) and without ($\tau_w = 0$) wall by assuming proportional control configuration combined of external active coils with the internal poloidal sensor. Plotted are [(a) and (c)] the mode eigenvalue and [(b) and (d)] the external tearing index.
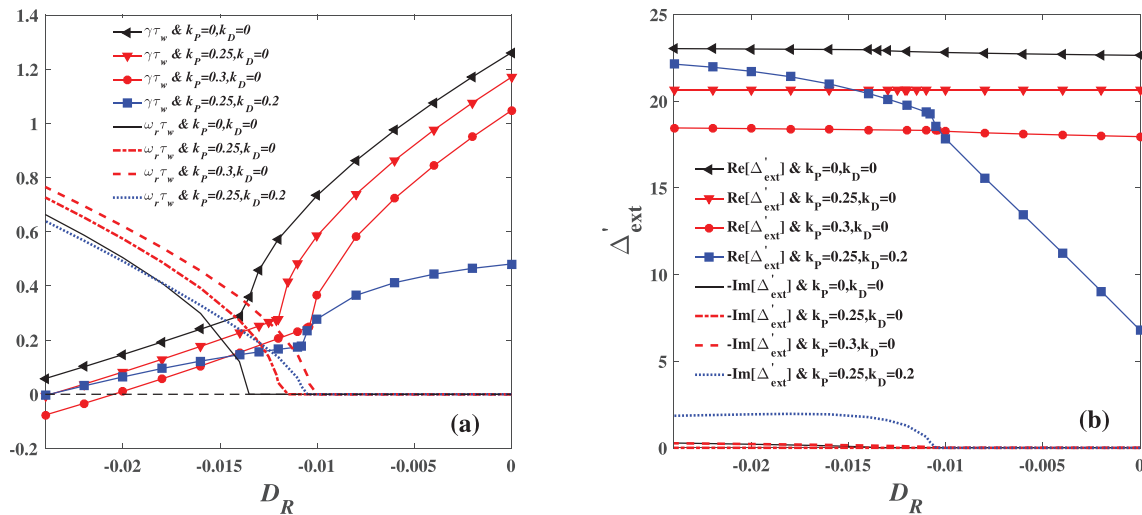
FIG. 8. Close-loop results for the $n = 1$ RP-EK with a resistive wall ($\tau_w = 10^4 \tau_A$) for (a) the mode eigenvalues and (b) the complex external tearing index, while scanning the proportional feedback gain and varying the value of the resistive interchange index $D_R = -0.001$–-0.014. Considered is a plasma with finite equilibrium pressure ($\beta = 0.05$). Assumed is a control scheme with the external active coil and the external poloidal sensor. The on-axis safety factor is fixed at $q_0 = 1.2$.

RP-EK can still be stabilized by the combination of external active coils and poloidal sensors (assuming the single-pole model), similar to that for the RP-EK with a resistive wall. A slight difference here is the less stabilization of the RP-EK in the presence of a resistive wall with the combination of external active coils and internal poloidal sensors. This is more evident from the comparison shown in Fig. 6. In the case of $\tau_w = 0$, the distinction between the external and internal (poloidal) sensors disappears since these two types of sensors refer to the relative radial position of the sensors to the wall. Therefore, the comparison of the close-loop RP-EK growth rates, between with and without wall, already shows that the presence of a resistive wall does affect the feedback results.

The next qualitative difference is that the corresponding close-loop Δ' remains real-valued with $\tau_w = 0$, whilst Δ' becomes complex-valued with a resistive wall [Figs. 6(c), 6(d), 7(c), and 7(d)]. This clearly shows that the presence of the wall eddy current dissipation can introduce imaginary part for the tearing index.

Finally, we point out that the difference between the no-wall and the resistive-wall results disappears at the marginal stability points [Figs. 6(a), 6(b), 7(a), and 7(b)] when the close-loop has zero mode frequency. This is understandable since the resistive wall eddy current completely disappears (thus recovering the no-wall case) at the marginal stability point with zero perturbation frequency. This is not the case with the inclusion of the GGJ-effect [Figs. 6(c), 6(d), 7(c), and 7(d)], where

FIG. 9. Open-loop and close-loop results for the $n = 1$ RP-EK for (a) the mode eigenvalue and (b) the complex external tearing index while scanning the resistive interchange index. Compared also are the results with proportional feedback and with PD-feedback. Considered is a plasma with finite equilibrium pressure $\beta = 0.05$. Assumed is the feedback configuration with the external active coil and the external poloidal sensor. The on-axis safety factor is fixed at $q_0 = 1.2$.

the mode has finite frequency at the marginal stability point. The marginal points, in terms of both the close-loop mode stability and the corresponding external tearing index, thus differ between the no-wall and the resistive wall cases.

Coming back to the case with finite wall time, the transition from the real to complex eigenvalue depends on the value of k_P and D_R, as shown in Fig. 8. When the absolute value of D_R is sufficiently small (e.g., $D_R = -0.001$), the eigenvalue of the RP-EK and the value of the corresponding Δ'_{ext} are all real. In addition, for the range of k_P between 0 and 0.25, Δ'_{ext} remains real independent of the choice for the D_R value.

In the presence of the GGJ effect, the derivative gain induced complex mode eigenvalue (and Δ'_{ext}) appears to be qualitatively different from that induced by the proportional action. This is demonstrated in Fig. 9, where we compare the P- and PD-control of the RP-EK while scanning the D_R value. The feedback scheme combines the external active coil and the external poloidal sensor. Apparently, with increasing D_R (toward the negative value), the growth rate of the RP-EK decreases [Fig. 9(a)]. The close-loop eigenvalue becomes complex at certain value of D_R. This transition occurs for both the open-loop and close-loop with either P- or PD-feedback, though at different D_R values.

The real part of the corresponding external tearing index Δ'_{ext} is independent of the resistive interchange index in the open-loop or close-loop with P-feedback. This implies that the RP-EK is controlled by the proportional feedback via modification of Δ'_{ext}, not via changing the inner layer physics. On the other hand, the same derivative action does result in different Δ'_{ext} while varying the D_R value. Figure 9(b) shows that, under the same derivative action, the external tearing index increases with increasing D_R (toward negative value), despite the fact that the growth rate of the RP-EK decreases. The effect of the derivative feedback action is thus non-trivial in terms of modifying the external tearing index. On the other hand, the P-feedback, with either $k_P = 0.25$ or $k_P = 0.3$, produces constant Δ'_{ext} values independent of D_R.

VI. CONCLUSIONS

Based on an analytic model, we have carried out systematic investigation of feedback control of the RP-RWM and RP-EK via the matching method [Eq. (14)]. The same method is also applied to study the IP-RWM as a special case, i.e., with vanishing inner layer tearing index at the mode rational surface. A key merit of the matching approach is that feedback modification of the external tearing index can be quantified by inserting the self-consistently calculated eigenvalue from the close-loop Eq. (14) back into expression (8) or (10). For the RP-RWM and RP-EK, the instability is controlled mainly via feedback modification of the external tearing index as demonstrated in this work.

Assuming six feedback coil configurations combining different types of active and sensor coils, we calculate modification of Δ'_{ext} by the P- or PD-control systems and map out the results in parameter spaces involving the proportional gain k_P, the derivative gain k_D, and the resistive interchange index D_R. We find that increasing either the proportional or derivative gain generally reduces Δ'_{ext} and stabilizes the RP-RWM or RP-EK with all six feedback configurations.

Feedback generally affects the external tearing index Δ'_{ext} independent of the inner layer physics, implying that feedback stabilizes the RP-RWM or RP-EK primarily via modification of the solution in the outer ideal region. One exception is the case where either sufficiently

large GGJ effect or strong control action produces a rotating instability in the static plasma. The close-loop external tearing index then becomes complex-valued due to the perturbed magnetic energy dissipation in the outer region, associated with the eddy current flowing in the resistive wall. The plasma inertia (again from the outer region) in principle plays a similar role as the wall eddy current, but the effect on Δ'_{ext} is several orders of magnitude weaker during feedback stabilization of the RP-RWM and RP-EK. For the latter, the inertia effect is already significantly reduced by plasma resistive damping in the open-loop.

With the single harmonic approximation, which is the constraint for the matching method, we find that the combination of external active coils and poloidal sensors often outperforms the other feedback configurations at large feedback gain. This counter-intuitive result is explained as the lack of (non-resonant) poloidal harmonics for proper description of the feedback coil geometry. This is confirmed by including multiple poloidal harmonics in the alternative control model based on the plasma response transfer function (the PRM model), which has previously been developed to study feedback control of the IP-RWM.

The fact that multiple poloidal harmonics are needed in order to better resolve the feedback coil geometry and thus to obtain quantitatively more correct results shows the drawback of the single-pole matching method employed in this study. Future work will exploit the possibility of multi-pole matching methods (as well as plasma flow) in conjunction with magnetic feedback. An alternative, which we also plan to pursue, is to study feedback modification of the tearing index utilizing toroidal codes. Nevertheless, we emphasize that most of the conclusions reached in this study still hold in the qualitative sense. In particular, we explicitly demonstrate that (i) magnetic feedback stabilizes the RP-RWM largely via modification of the external tearing index, (ii) magnetic feedback generally stabilizes the RP-RWM and RP-EK with various feedback coil configurations, and (iii) feedback can induce a complex external tearing index, due to the wall eddy current energy dissipation.

This work provides a theoretical basis for interpreting the experimental results of magnetic feedback control of resistive-plasma instabilities in fusion devices. Compared to the previous analytic work, we show a clear separation of the feedback effect on the outer and inner regions via the matching method. This is of fundamental importance since magnetic feedback is not expected to help control an instability which is "interior" to the plasma. In other words, magnetic feedback, based on coils outside the plasma, cannot be effective if the required action is primarily targeting the inner resistive layer. Our findings also suggest a way of quantifying the feedback action on the resistive modes in modeling with toroidal codes. More specifically, it will be extremely useful if a toroidal code simulation can extract the modification of the tearing index by magnetic feedback. This subsequently allows (i) separating the feedback problem into two independent problems for the outer and inner regions; (ii) verifying whether our analytic approach (and the associated assumptions) is qualitatively reasonable; and (iii) verifying certain physics consequences such as whether the resistive wall eddy currents can indeed induce a complex tearing index.

As already implied above, our approach can also be applied to study magnetic control of other MHD modes, in particular, the TM and NTM. Conventionally, NTM is controlled by non-magnetic means such as the electron cyclotron current drive. Magnetic control can provide a complementary method as long as feedback can help to modify (reduce) the external tearing index.

ACKNOWLEDGMENTS

APPENDIX A: SPECIAL CASES OF IP-RWM

This appendix lists simplified versions for the open-loop and close-loop growth rates of the IP-RWM in special cases. The open-loop growth rate of the IP-RWM is derived from Eq. (6),

$$\gamma_{\mathrm{nf}}\tau_w = -2m\frac{1-(m-nq_0)}{1-(r_0/r_w)^{2m}-(m-nq_0)}. \tag{A1}$$

For the plasma with vanishing equilibrium pressure ($\beta = 0$), the close-loop growth rate with the P-controller can be straightforwardly obtained for the IP-RWM, assuming various combinations of the active and sensor coil types

$$\gamma\tau_w = \begin{cases} -2mk_P + C_1 & ext.coil + rad.sensor, \\ (-C_2mk_P + C_1)/(1-2mk_P) & ext.coil + ext.pol.sensor, \\ -C_2mk_P + C_1 & ext.coil + int.pol.sensor, \\ -C_3k_P + C_1 & int.coil + rad.sensor, \\ -C_3mk_P + C_1 & int.coil + ext.pol.sensor, \\ (-C_3mk_P + C_1)/(1+C_3k_P) & int.coil + int.pol.sensor, \end{cases} \tag{A2}$$

where $C_1 = \gamma_{\mathrm{nf}}\tau_w$, $C_2 = -2m\frac{1-(m-nq_0)+(r_0/r_w)^{2m}}{1-(m-nq_0)-(r_0/r_w)^{2m}}$ and $C_3 = 2m\frac{1-(m-nq_0)-(r_0/r_f)^{2m}}{1-(m-nq_0)-(r_0/r_w)^{2m}}$ are all positive constants.

Assuming the combination of internal active coils and the radial sensor, the close-loop growth rate with a PD-control is calculated as

$$\gamma\tau_w = \frac{-C_3k_P + C_1}{-C_4k_D + 1}, \tag{A3}$$

where $C_4 = -\frac{2m[1-(m-nq_0)]-(r_0/r_f)^{2m}}{1-(m-nq_0)-(r_0/r_w)^{2m}}$ is also a positive constant.

APPENDIX B: ALTERNATIVE APPROACH TO STUDY IP-RWM FEEDBACK

This appendix exploits the PRM approach for feedback control of the IP-RWM in order to compare with the matching approach adopted in the main part of this work and to explain certain counter-intuitive results obtained with the matching approach. Specifically, Sec. III finds that the combination of the external active coil and the poloidal sensor provides more efficient control at large proportional gain than the internal active coil.

Below we repeat the key steps in deriving the PRM model.[28–30] For each poloidal harmonic m, the corresponding transfer function $M^m(s)$, from the control current to the sensor signal, is obtained for the same equilibrium (with vanishing pressure) as specified in Sec. II.

(i) The perturbed radial field component b_r satisfies the ideal MHD force balance condition at the plasma boundary surface $r = a+$,

$$\left.\frac{rb'_r}{b_r}\right|_{a+} = C, \tag{B1}$$

where C is a constant independent of feedback.

(ii) The wall equation (thin wall is assumed)

$$\left.\frac{r[b'_r]}{b_r}\right|_{r_w} = 2s, \tag{B2}$$

where $s = \gamma\tau_w$ is the growth rate of the RWM with feedback.

(iii) The total field in various vacuum regions outside the plasma can be written as the sum of contributions from the plasma, the wall, and the active coil currents

$$b_r = b_r^p\left(\frac{r}{a}\right)^{sgn(a-r)\mu-1} + b_r^w\left(\frac{r}{r_w}\right)^{sgn(r_w-r)\mu-1} + b_r^f\left(\frac{r}{r_f}\right)^{sgn(r_f-r)\mu-1}. \tag{B3}$$

The above three conditions yield a relation

$$\frac{\mu-1-C}{\mu+1+C}\left(\frac{a}{r_w}\right)^{2\mu} = -\frac{\gamma_{nf}\tau_w + \mu}{\gamma_{nf}\tau_w}, \tag{B4}$$

where $\gamma_{nf}\tau_w = -\mu\frac{1\mp(m-nq_0)}{1\mp(m-nq_0)-(r_0/r_w)^{2\mu}}$ is the growth rate of the ideal external kink mode, with $\mu = |m|$ and $\mp$ stands for $-sgn(m)$.

Define the open-loop transfer function for the radial and poloidal sensors as

$$M_r^m(s) \equiv \frac{b_r^s}{b_r^f} \tag{B5}$$

and

$$M_\theta^m(s) \equiv \frac{jb_\theta^s|_{r_s}}{b_r^f}, \quad b_\theta^s|_{r_s} = \frac{j}{m}\left(rb_r^s\right)'|_{r_s} \tag{B6}$$

respectively, where b_r^s is the total radial field at the sensor position, which is assumed to be the wall radial position. Considering various combinations of the active and sensor coil types, the transfer functions for the radial and poloidal sensors are obtained by expressing b_r^p, b_r^w and b_r^s via b_r^f, yielding

$$M_r^m(s) = \begin{cases} \dfrac{\alpha}{s - \gamma_{nf}\tau_w} & (r_f < r_w), \\ \dfrac{\beta}{s - \gamma_{nf}\tau_w} & (r_w < r_f), \end{cases} \tag{B7}$$

$$M_\theta^m(s) = \begin{cases} \dfrac{\mu + 2s}{m(s - \gamma_{nf}\tau_w)}\alpha & (r_f < r_s < r_w), \\[2mm] \dfrac{\mu}{m(s - \gamma_{nf}\tau_w)}\alpha & (r_f < r_w < r_s), \\[2mm] \dfrac{\mu\lambda}{m(s - \gamma_{nf}\tau_w)} & (r_s < r_w < r_f), \\[2mm] \dfrac{\mu(\lambda - 2\kappa s)}{m(s - \gamma_{nf}\tau_w)} & (r_w < r_s < r_f), \end{cases} \qquad (B8)$$

where

$$\begin{cases} \alpha = \mu(r_w/r_f)^{\mu-1} + \gamma_{nf}\tau_w[(r_w/r_f)^{\mu-1} - (r_w/r_f)^{-\mu-1}], \\ \beta = \mu(r_w/r_f)^{\mu-1}, \\ \lambda = 2\gamma_{nf}\tau_w(r_w/r_f)^{\mu-1} + \mu(r_w/r_f)^{\mu-1}, \\ \kappa = (r_w/r_f)^{\mu-1}. \end{cases}$$

The open-loop total transfer functions[29] for different poloidal harmonics are coupled via a window-pane representation of the active coils and the point-wise sensor signal (for either the radial or poloidal sensors), resulting in a total transfer function of

$$P(s) = \sum_m M^m(s)f_m \exp(jm\theta_c)\exp(jm\theta_s),$$

where θ_c (θ_s) is the poloidal angle of the center of the active (sensor) coil locations, and f_m is the geometrical coupling factor

$$f_m = \frac{m}{2\mu}\frac{\sin(m\theta_f)}{\sin\theta_f}\frac{r_w^2 + r_f^2 - 2r_wr_f\cos\theta_f}{r_f^2}$$

with θ_f being the half-width of the poloidal coverage by the active coils. Here, we consider one set of feedback and sensor coils, both placed at the low field side near the outboard mid-plane.
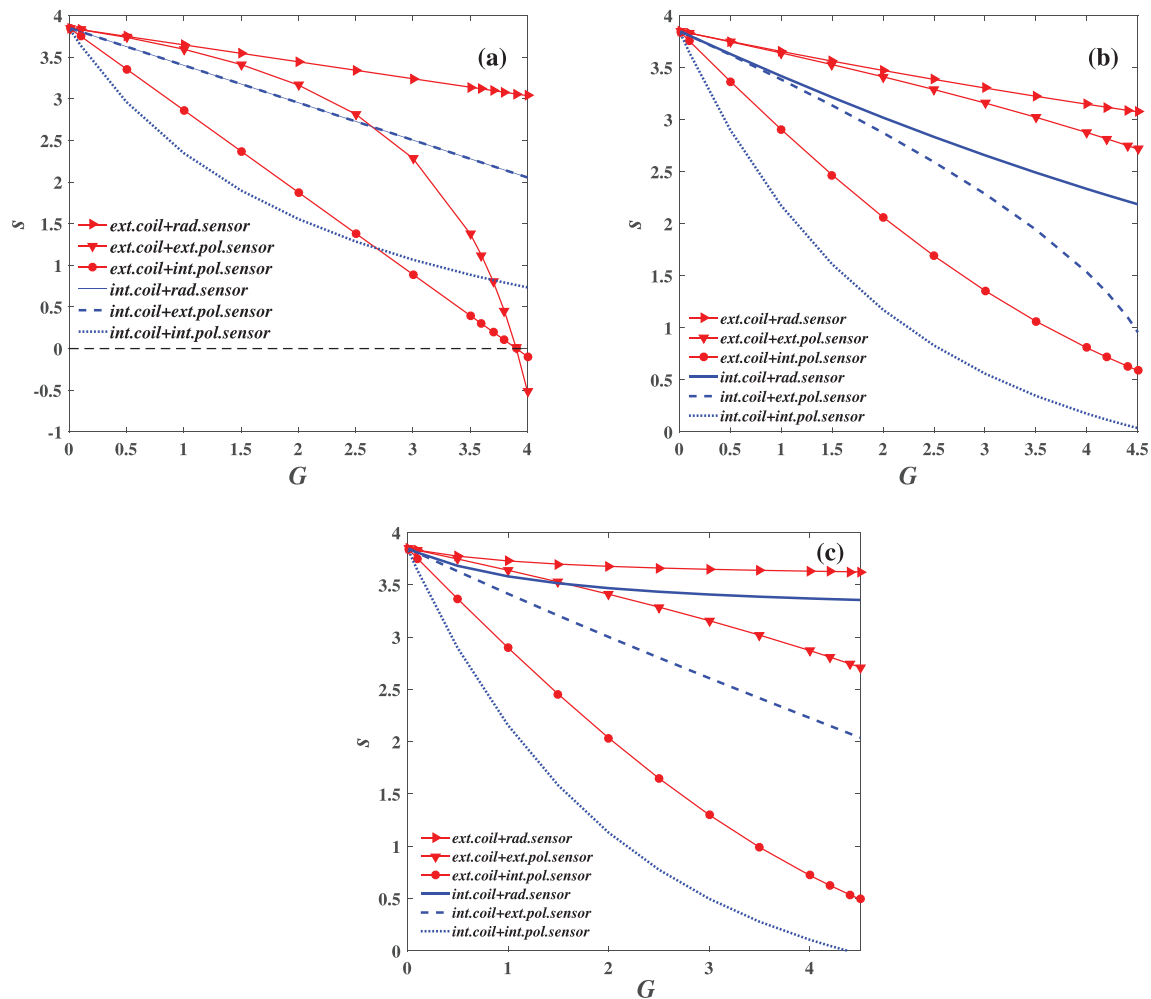
FIG. 10. The growth rates of the $n = 1$ IP-RWM vs the feedback gain, assuming various combinations of the active and sensor coil types. The poloidal coverage by the active coil is fixed $\theta_f = \pi/9$. (a) single-m poloidal harmonic ($m = 2$), (b) two poloidal harmonics ($m = \pm 2$) and (c) multiple poloidal harmonics ($m = -10$–~ 10) are considered in the transfer function P(s), respectively.

With a proportional controller and feedback gain G, the close-loop eigenvalue is determined by the solution of the characteristic equation

$$1 + GP(s) = 0. \tag{B9}$$

Taking the single-m poloidal harmonic approximation, the close-loop eigenvalue is readily calculated

$$s = \begin{cases} \gamma_{nf}\tau_w - H\beta & ext.coil + rad.sensor, \\ \dfrac{m\gamma_{nf}\tau_w - H\lambda\mu}{m - 2H\kappa\mu} & ext.coil + ext.pol.sensor, \\ \dfrac{m\gamma_{nf}\tau_w - H\lambda\mu}{m} & ext.coil + int.pol.sensor, \\ \gamma_{nf}\tau_w - H\alpha & int.coil + rad.sensor, \\ \dfrac{m\gamma_{nf}\tau_w - H\alpha\mu}{m} & int.coil + ext.pol.sensor, \\ \dfrac{m\gamma_{nf}\tau_w - H\alpha\mu}{m + 2H\alpha} & int.coil + int.pol.sensor, \end{cases} \tag{B10}$$

where $H = f_m G$ for the single row of active coils and sensor coils located at the outboard mid-plane ($\theta_c = 0$ and $\theta_s = 0$). It is evident that the PRM approach yields the same feedback result, (B10), as that from the matching approach from the IP-RWM [setting expression (8) = 0], i.e., (A2) from Appendix A. The difference in the coefficients comes from different definition of the control signals.

The above expression (B10) [or equivalently expression (A2)] shows that a P-control with the internal active coil and the internal poloidal sensor provides more stabilization than that of the external active coil ($\frac{m\gamma_{nf}\tau_w - H\lambda\mu}{m} > \frac{m\gamma_{nf}\tau_w - H\alpha\mu}{m+2H\alpha}$) if the feedback gain is sufficiently small $0 < H < \frac{\gamma_{nf}\tau_w+1}{\lambda} - \frac{1}{\alpha}$. However, at large feedback gain $H > \frac{\gamma_{nf}\tau_w+1}{\lambda} - \frac{1}{\alpha}$, the external active coil becomes more

effective ($\frac{m\gamma_{nf}\tau_w - H\lambda\mu}{m} < \frac{m\gamma_{nf}\tau_w - H\alpha\mu}{m+2H\alpha}$). These results are also plotted in Fig. 10(a).

On the other hand, we can also numerically solve Eq. (B9) by including two harmonics ($m = \pm 2$) or even multiple harmonics ($m = -10 \sim 10$) in the transfer function $P(s)$. The calculated close-loop growth rates for the IP-RWM are plotted in Figs. 10(b) and 10(c), respectively. In both cases, we find that the internal active coil provides stronger stabilization to the mode than the external active coil, independent of the proportional feedback gain value.

## APPENDIX C: EFFECTS OF DERIVATIVE CONTROL ACTION

Active control of the IP-RWM, RP-RWM, and RP-EK with proportional–derivative feedback is discussed below. For each type of instability, we shall consider expression (10), instead of expression (8) which is valid for the proportional controller. We shall vary the derivative gain k_D at fixed proportional gain.

1. Control of IP-RWM with PD-feedback

We again numerically solve the IP-RWM dispersion relation $\Delta'_{ext,PD}(K, \gamma) = 0$ [i.e., expression (10) = 0] with PD-feedback. The results are reported in Fig. 11, again assuming various combinations of the active and sensor coil types. For both plasmas (with vanishing or finite equilibrium pressure), the derivative action reduces the mode growth rate, except the case of internal active coil combined with the radial sensor. The latter, somewhat surprising, result can be analytically understood. For this specific case, the growth rate of the close-loop system becomes $\gamma\tau_w = (-C_3 k_P + C_1)/(-C_4 k_D + 1)$ with vanishing equilibrium pressure $\beta = 0$ [Eq. (A3), Appendix A]. At fixed proportional gain of $k_P = 0.1$, the numerator $-C_3 k_P + C_1 > 0$. Since $C_4 > 0$, increasing derivative gain (up to certain limit) also increases the mode growth rate.
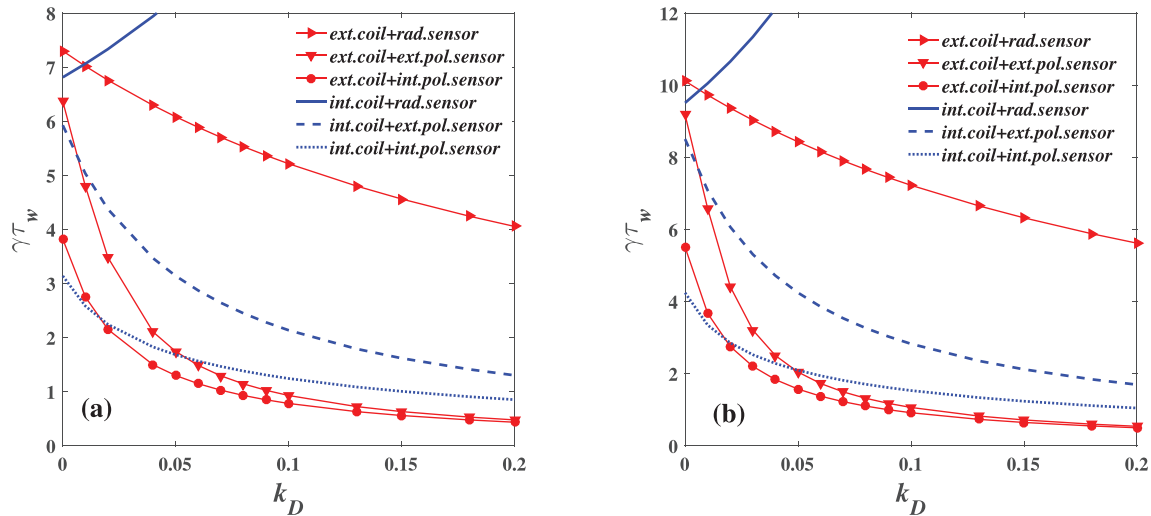
FIG. 11. The growth rate of the $n = 1$ IP-RWM vs the derivative gain, assuming various combinations of the active and sensor coil types. The proportional feedback gain is fixed at $k_P = 0.1$. Considered are two equilibria with either (a) vanishing pressure $\beta = 0$ or (b) finite pressure $\beta = 0.03$. The on-axis safety factor is fixed at $q_0 = 1.05$.
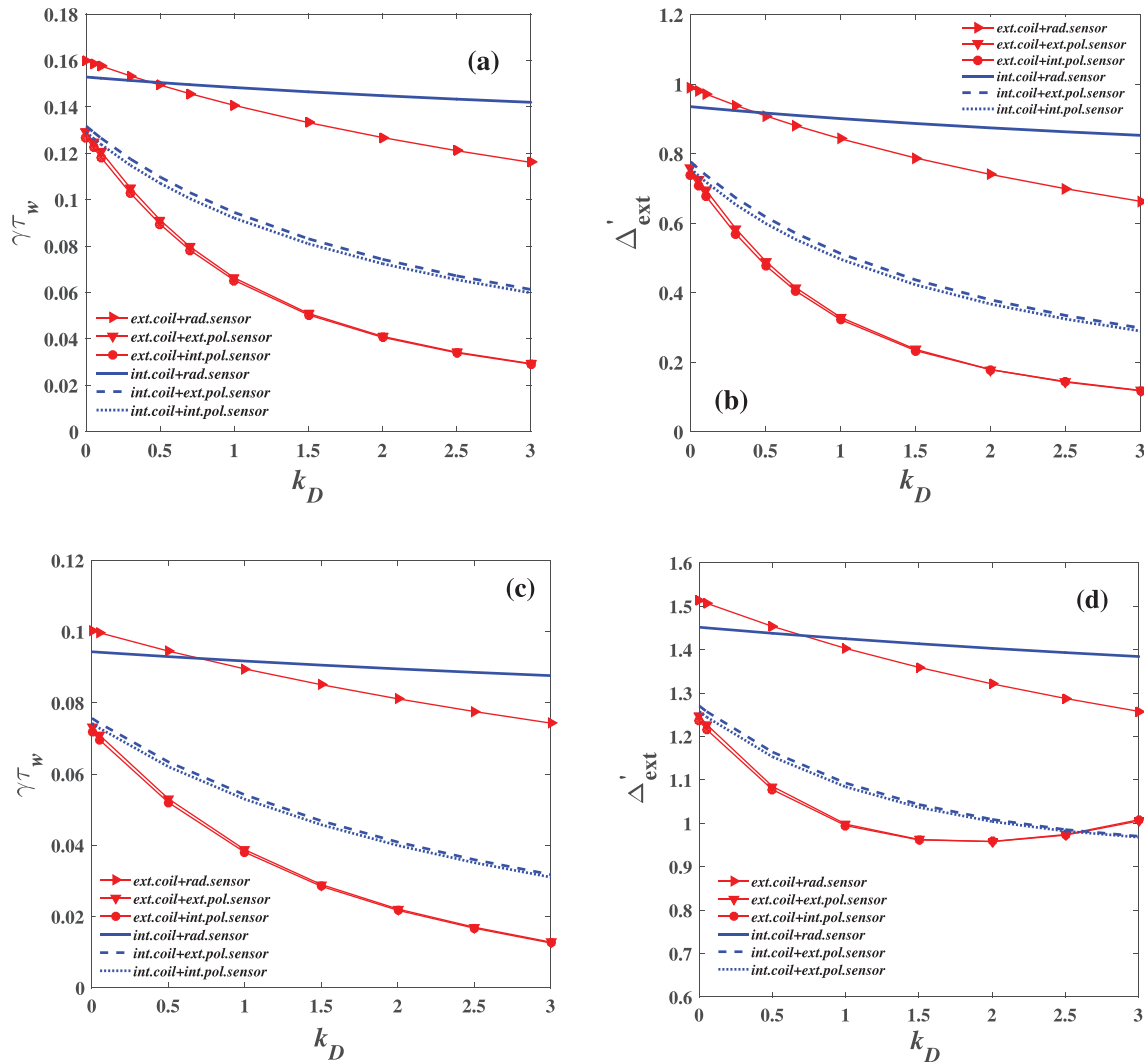
FIG. 12. Close-loop results for the $n = 1$ RP-RWM, assuming equilibria with [(a) and (b)] vanishing pressure $\beta = 0$, and [(c) and (d)] finite pressure $\beta = 0.03$ with the GGJ included into the inner layer tearing index ($D_R = -0.0003$). Compared are the results with various feedback coil configurations while scanning the derivative gain. The proportional gain is fixed at $k_P = 0.1$. Plotted are [(a) and (c)] the mode growth rate and [(b) and (d)] the external tearing index. The on-axis safety factor is fixed at $q_0 = 1.05$.

We note that the IP-RWM cannot be fully stabilized by the derivative action. At fixed proportional gain, the mode growth rate approaches a positive constant at infinite derivative gain. This is understandable since the stabilizing effect of the derivative action diminishes as the mode approaches the marginal stability point (at vanishing mode frequency).

2. Control of RP-RWM with PD-feedback

We now solve Eq. (14) but with the external tearing index defined by expression (10). The results are presented in Fig. 12, without [(a) and (b)] or with [(c) and (d)] the GGJ effect. Note that the general trend remains similar between the two cases (with or without the GGJ effect). For the case with the GGJ effect [(c) and (d)], the proportional gain is chosen such that the close-loop eigenvalue is real at vanishing derivative gain. The latter, when introduced, does not yield finite mode frequency.

The feedback results with either external or internal poloidal sensors remain similar while scanning the derivative gain. This is largely because the mode growth is already weak at $k_P = 0.1$ and $k_D = 0$. A weakly growing instability does not introduce large eddy current in the resistive wall. We also note that the derivative gain is stabilizing with all types of feedback coil configurations, including the combination of internal active coils and the radial sensor (albeit with very weak effect).

Similar to the case for the IP-RWM, the derivative action does not fully stabilize the RP-RWM. Both the mode growth rate and the external tearing index tend to saturate at large k_D values.

3. Control of RP-EK with PD-feedback

Figure 13 reports the PD feedback results by numerically solving Eq. (14), which links expression (10) with (12) or (13), while
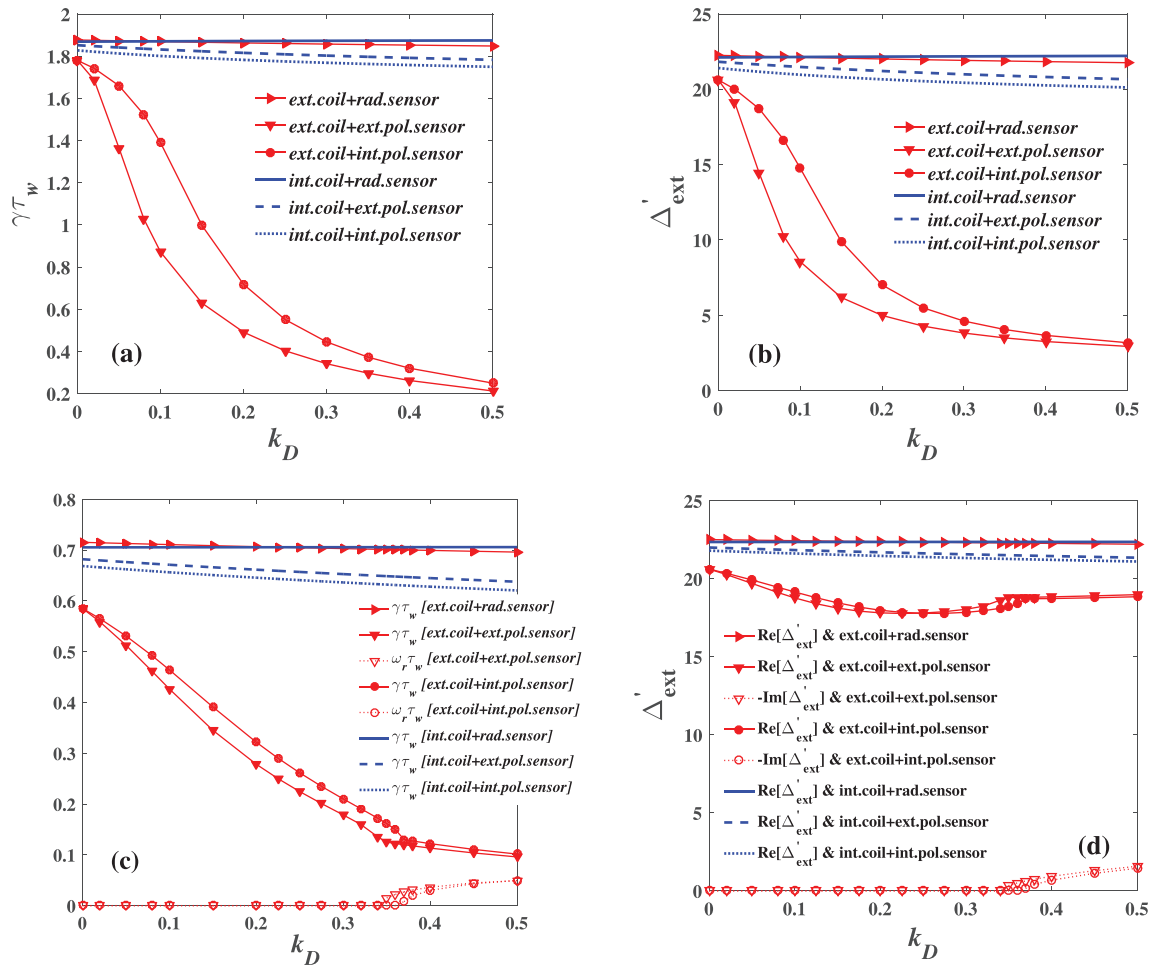
FIG. 13. Close-loop results for the $n = 1$ RP-EK, assuming equilibria with [(a) and (b)] vanishing pressure $\beta = 0$ and [(c) and (d)] finite pressure $\beta = 0.05$ with the GGJ included into the inner layer tearing index ($D_R = -0.01$). Compared are results with various feedback coil configurations while scanning the derivative gain. The proportional gain is fixed at $k_P = 0.25$. Plotted are [(a) and (c)] the mode eigenvalue and [(b) and (d)] the complex external tearing index. The on-axis safety factor is fixed at $q_0 = 1.2$.

scanning the derivative gain k_D at fixed proportional gain of $k_P = 0.25$. Among various combinations of the active and sensor coils, the external active coil, combined with poloidal sensors, stands out as the most effective one in reducing the mode growth rate by the derivative action. An interesting new observation here is that, for the RP-EK, the derivative action at large gain value can also introduce complex close-loop eigenvalue [Fig. 13(c)] and complex Δ'_{ext} [Fig. 13(d)]. Moreover, the real part of Δ'_{ext} increases with increasing the derivative (at large gain values). This is in contrast to the monotonic decrease in the mode growth rate with increasing k_D.

DATA AVAILABILITY

The data that support the findings of this study are available from the corresponding author upon reasonable request.

REFERENCES

[1]T. C. Hender, J. C. Wesley, J. Bialek, A. Bondeson, A. H. Boozer, R. J. Buttery, A. Garofalo, T. P. Goodman, R. S. Granetz, Y. Gribov, O. Gruber, M. Gryaznevich, G. Giruzzi, S. G€unter, N. Hayashi, P. Helander, C. C. Hegna, D. F. Howell, D. A. Humphreys, G. T. A. Huysmans, A. W. Hyatt, A. Isayama, S. C. Jardin, Y. Kawano, A. Kellman, C. Kessel, H. R. Koslowski, R. J. L. Haye, E. Lazzaro, Y. Q. Liu, V. Lukash, J. Manickam, S. Medvedev, V. Mertens, S. V. Mirnov, Y. Nakamura, G. Navratil, M. Okabayashi, T. Ozeki, R. Paccagnella, G. Pautasso, F. Porcelli, V. D. Pustovitov, V. Riccardo, M. Sato, O. Sauter, M. J. Schaffer, M. Shimada, P. Sonato, E. J. Strait, M. Sugihara, M. Takechi, A. D. Turnbull, E. Westerhof, D. G. Whyte, R. Yoshino, H. Zohm, and ITPA MHD Disruption and Magnetic Control Topical Group, Nucl. Fusion **47**, S128 (2007).
[2]M. S. Chu and M. Okabayashi, Plasma Phys. Controlled Fusion **52**, 123001 (2010).
[3]F. Troyon, R. Gruber, H. Saurenmann, S. Semenzato, and S. Succi, Plasma Phys. Controlled Fusion **26**, 209 (1984).
[4]A. Bondeson and D. Ward, Phys. Rev. Lett. **72**, 2709 (1994).
[5]M. S. Chu, J. M. Greene, T. H. Jensen, R. L. Miller, A. Bondeson, R. W. Johnson, and M. E. Mauel, Phys. Plasmas **2**, 2236 (1995).
[6]R. Betti and J. P. Freidberg, Phys. Rev. Lett. **74**, 2949 (1995).
[7]R. Fitzpatrick and A. Y. Aydemir, Nucl. Fusion **36**, 11 (1996).
[8]J. R. Drake, P. R. Brunsell, D. Yadikin, M. Cecconello, J. A. Malmberg, D. Gregoratto, R. Paccagnella, T. Bolzonella, G. Manduchi, L. Marrelli, S.

Ortolani, G. Spizzo, P. Zanca, A. Bondeson, and Y. Q. Liu, Nucl. Fusion **45**, 557 (2005).

[9]V. D. Pustovitov, Nucl. Fusion **55**, 033008 (2015).

[10]J. M. Finn, Phys. Plasmas **2**, 198 (1995).

[11]J. M. Finn, Phys. Plasmas **2**, 3782 (1995).

[12]A. Bondeson, C. G. Gimblett, and R. J. Hastie, Phys. Plasmas **6**, 637 (1999).

[13]Y. L. He, Y. Q. Liu, Y. Liu, G. Z. Hao, and A. K. Wang, Phys. Rev. Lett. **113**, 175001 (2014).

[14]Y. L. He, Y. Q. Liu, Y. Liu, C. Liu, G. L. Xia, A. K. Wang, G. Z. Hao, L. Li, and S. Y. Cui, Phys. Plasmas **23**, 012506 (2016).

[15]S. X. Yang, Y. Q. Liu, G. Z. Hao, Z. X. Wang, Y. L. He, H. D. He, A. K. Wang, and M. Xu, Phys. Plasmas **25**, 012125 (2018).

[16]Y. Q. Liu and A. Bondeson, Phys. Rev. Lett. **84**, 907 (2000).

[17]S. Sabbagh, R. Bell, J. Menard, D. Gates, A. Sontag, J. Bialek, B. LeBlanc, F. Levinton, K. Tritz, and H. Yuh, Phys. Rev. Lett. **97**, 045004 (2006).

[18]Y. Q. Liu, M. S. Chu, I. T. Chapman, and T. C. Hender, Phys. Plasmas **15**, 112503 (2008).

[19]G. L. Xia, Y. Liu, and Y. Q. Liu, Plasma Phys. Controlled Fusion **56**, 095009 (2014).

[20]G. L. Xia, Y. Q. Liu, C. J. Ham, S. Wang, L. Li, G. Y. Zheng, J. X. Li, N. Zhang, X. Bai, G. Q. Dong, and HL-2M team, Nucl. Fusion **59**, 016017 (2019).

[21]S. Wang, Y. Q. Liu, G. Y. Zheng, X. M. Song, G. Z. Hao, G. L. Xia, L. Li, B. Li, N. Zhang, G. Q. Dong, and X. Bai, Nucl. Fusion **59**, 096021 (2019).

[22]J. M. Finn, Phys. Plasmas **13**, 082504 (2006).

[23]D. P. Brennan and J. M. Finn, Phys. Plasmas **21**, 102507 (2014).

[24]P. Zanca, R. Paccagnella, C. Finotti, A. Fassina, G. Manduchi, R. Cavazzana, P. Franz, C. Piron, and L. Piron, Nucl. Fusion **55**, 043020 (2015).

[25]Y. S. Park, S. A. Sabbagh, J. H. Ahn, B. H. Park, H. S. Kim, J. W. Berkery, J. M. Bialek, Y. Jiang, J. G. Bak, A. H. Glasser, J. S. Kang, J. Lee, H. S. Han, S. H.

Hahn, Y. M. Jeon, J. G. Kwak, H. K. Park, Z. R. Wang, J.-K. Park, N. M. Ferraro, and S. W. Yoon, Nucl. Fusion **60**, 056007 (2020).

[26]L. Pigatto, N. Aiba, T. Bolzonella, N. Hayashi, M. Honda, Y. Q. Liu, G. Marchiori, S. Mastrostefano, G. Matsunaga, M. Takechi, and F. Villone, Nucl. Fusion **59**, 106028 (2019).

[27]E. J. Strait, J. L. Barr, M. Baruzzo, J. W. Berkery, R. J. Buttery, P. C. de Vries, N. W. Eidietis, R. S. Granetz, J. M. Hanson, C. T. Holcomb, D. A. Humphreys, J. H. Kim, E. Kolemen, M. Kong, M. J. Lanctot, M. Lehnen, E. Lerche, N. C. Logan, M. Maraschek, M. Okabayashi, J. K. Park, A. Pau, G. Pautasso, F. M. Poli, C. Rea, S. A. Sabbagh, O. Sauter, E. Schuster, U. A. Sheikh, C. Sozzi, F. Turco, A. D. Turnbull, Z. R. Wang, W. P. Wehner, and L. Zeng, Nucl. Fusion **59**, 112012 (2019).

[28]A. Bondeson, Y. Q. Liu, D. Gregoratto, Y. Gribov, and V. D. Pustovitov, Nucl. Fusion **42**, 768 (2002).

[29]Y. Q. Liu, Plasma Phys. Controlled Fusion **48**, 969 (2006).

[30]J. Ren, Y. Q. Liu, Y. Liu, and S. Y. Medvedev, Nucl. Fusion **58**, 126017 (2018).

[31]A. Bondeson and H. X. Xie, Phys. Plasmas **4**, 2081 (1997).

[32]H. P. Furth, J. Killeen, and M. N. Rosenbluth, Phys. Fluids **6**, 459 (1963).

[33]A. H. Glasser, J. M. Greene, and J. L. Johnson, Phys. Fluids **18**, 875 (1975).

[34]Y. Q. Liu, R. J. Hastie, and T. C. Hender, Phys. Plasmas **19**, 092510 (2012).

[35]B. Coppi, R. Galvao, R. Pellat, M. N. Rosenbluth, and P. H. Rutherford, Fiz. Plazmy **2**, 961 (1976) [Sov. J. Plasma Phys. **2**, 533 (1976)].

[36]A. H. Glasser, J. M. Greene, and J. L. Johnson, Phys. Fluids **19**, 567 (1976).

[37]Y. Q. Liu, J. W. Connor, S. C. Cowley, C. J. Ham, R. J. Hastie, and T. C. Hender, Phys. Plasmas **19**, 072509 (2012).

[38]R. Fitzpatrick and T. H. Jensen, Phys. Plasmas **3**, 2641 (1996).

[39]M. Okabyashi, N. Pomphrey, and R. E. Hatcher, Nucl. Fusion **38**, 1607 (1998).

[40]D. P. Brennan, E. J. Strait, A. D. Turnbull, M. S. Chu, R. J. La Haye, T. C. Luce, T. S. Taylor, S. Kruger, and A. Pletzer, Phys. Plasmas **9**, 2998 (2002).

[41]R. Betti, Phys. Plasmas **5**, 3615 (1998).